Table 1 *Continued*

	Name	Accession No.	Categories	Fraction
110	Tropomyosin γ	Q8K0Z5	Other-cytoskeleton	E
111	Type II brain 4.1	Q9JMB3	Other-cytoskeleton	S
112	Vimentin	P08670	Other-cytoskeleton	S, E
113	Wasp family 1	Q8R5H6	Other-cytoskeleton	S
114	M-phase phosphoprotein 1	Q96Q89	Motor	E
115	Myosin Va	Q9Y4I1	Motor	E
116	Myosin Vb	Q9ULV0	Motor	S
117	Myosin, heavy polypeptide 10	P35580	Motor	S
118	Myosin, heavy polypeptide 11	O08638	Motor	S, E
119	Myosin, heavy polypeptide 13	Q9GJP9	Motor	E
120	Myosin, heavy polypeptide 14	Q7Z406	Motor	S
121	Myosin, heavy polypeptide 16	Q9H6N6	Motor	E
122	Myosin, heavy polypeptide 7	Q91Z83	Motor	E
123	Myosin, heavy polypeptide 9	P35579	Motor	S, E
124	AKAP 450	Q99996	Centrosome	S
125	Centrosomal protein Cep290	O15078	Centrosome	S, E
126	Oral–facial–digital syndrome 1 protein	O75665	Centrosome	E
127	Rootletin	CROCC	Centrosome	E
128	78 kDa glucose-regulated protein	P34935	Chaperone	S, E
129	DnaJ (Hsp40) homologue, subfamily A, member 2	Q9QYJ0	Chaperone	E
130	DnaJ (Hsp40) homologue, subfamily B, member 14	Q8TBM8	Chaperone	E
131	Heat shock cognate 71 kDa protein	P11142	Chaperone	S, E
132	Heat shock protein HSP 90-α	P07901	Chaperone	S
133	Heat shock-related 70 kDa protein 2	P54652	Chaperone	E
134	Heat shock-related 70 kDa protein 4	O88600	Chaperone	S
135	Orp150 (150 kDa oxygen-regulated protein precursor)	Q63617	Chaperone	S
136	Stress-induced-phosphoprotein 1	O35814	Chaperone	S
137	THEG protein	Q9P2T0	Chaperone	S
138	Giantin	Q14789	Golgi	E
139	Golgin-245	Q13439	Golgi	S, E
140	Optineurin	Q96CV9	Golgi	S
141	PACS-1	O88588	Golgi	S
142	Rat GCP360	Q63714	Golgi	E
143	ADP–ATP translocase 3	P32007	Mitochondria	E
144	ADP–ATP translocase 4	Q9H0C2	Mitochondria	E
145	ATPase inhibitor precursor, mitochondrial	Q9UII2	Mitochondria	S
146	Mitochondrial ribosomal protein L51	Q9CPY1	Mitochondria	S
147	Peroxiredoxin V (PrxV) protein	Q9JHL8	Mitochondria	S
148	Solute carrier family 25, member 5	Q545A2	Mitochondria	S
149	Vacuolar adenosine triphosphatase subunit A	P50516	Mitochondria	S
150	APEX nuclease	P27695	NA-binding	S
151	Cell growth regulating nucleolar protein LYAR	Q08288	NA-binding	S
152	DEAD box polypeptide 27	Q96GQ7	NA-binding	E
153	DEAD box protein RB	Q92499	NA-binding	S
154	DNA cytosine methyltransferase 3α	Q9Y6K1	NA-binding	E
155	DNA polymerase κ	Q9UBT6	NA-binding	S
156	DNA repair protein RAD50	P70388	NA-binding	E
157	DNA topoisomerase I	Q07050	NA-binding	E
158	DNA topoisomerase IIα	O55078	NA-binding	E
159	DNA-dependent ATPase SNF2L	Q6PGB8	NA-binding	E
160	ETOILE	Q9R226	NA-binding	E
161	Heat shock transcription factor 2	Q9BS48	NA-binding	E
162	Heterogeneous nuclear ribonucleoprotein A1	P09651	NA-binding	S
163	Heterogeneous nuclear ribonucleoprotein A2/B	O88569	NA-binding	S
164	Heterogeneous nuclear ribonucleoprotein A3	Q8BG05	NA-binding	S

Continued overleaf

© 2008 The Authors
Journal compilation © 2008 by the Molecular Biology Society of Japan/Blackwell Publishing Ltd.

Table 1 *Continued*

	Name	Accession No.	Categories	Fraction
165	Heterogeneous nuclear ribonucleoprotein G	O97560	NA-binding	S
166	Heterogeneous nuclear ribonucleoprotein K	P61978	NA-binding	E
167	Heterogeneous nuclear ribonucleoprotein M	Q9D0E1	NA-binding	S, E
168	Heterogeneous nuclear ribonucleoprotein R	Q99KG1	NA-binding	E
169	Heterogeneous nuclear ribonucleoprotein U	Q63555	NA-binding	S, E
170	Homeobox protein TGIF2LX	Q8MID8	NA-binding	S
171	KH domain containing, RNA binding, signal transduction-associated 1	Q07666	NA-binding	E
172	KRAB-A interacting protein	Q62318	NA-binding	S
173	LLDBP	Q14756	NA-binding	S
174	Microphthalmia-associated transcription factor	O88368	NA-binding	S
175	Minor histocompatibility antigen HA-8	Q15397	NA-binding	E
176	Myelin transcription factor 1-like protein	Q9UL68	NA-binding	S
177	Non-POU-domain-containing, octamer binding protein	Q99K48	NA-binding	S
178	Nucleolar transcription factor 1	P25977	NA-binding	S
179	Origin recognition complex subunit 1	Q9JI69	NA-binding	S
180	Plasminogen activator inhibitor 1 RNA-binding protein	Q8NC51	NA-binding	S, E
181	RENT1	Q9EPU0	NA-binding	S
182	Ribonuclease 4	P34096	NA-binding	S
183	RNA-binding protein 27	Q5SFM8	NA-binding	S
184	RNA-binding protein 5	P52756	NA-binding	E
185	RNA-binding protein 6	P78332	NA-binding	S
186	SOX-10	P56693	NA-binding	E
187	SOX-21	Q811W0	NA-binding	E
188	Splicing co-activator subunit SRm300	Q9UQ35	NA-binding	S
189	Splicing factor 3 subunit 1	Q8K4Z5	NA-binding	E
190	Splicing factor, arginine/serine-rich 6	Q6GL71	NA-binding	S
191	Splicing factor, proline- and glutamine-rich, SFPQ	Q8VIJ6	NA-binding	S, E
192	Structural maintenance of chromosome 1-like 1 protein	Q9CU62	NA-binding	S, E
193	Structural maintenance of chromosome 2-like 1 protein	O95347	NA-binding	S
194	Structural maintenance of chromosomes 5-like 1	Q8CG46	NA-binding	E
195	Structural maintenance of chromosomes 6-like 1	Q96SB8	NA-binding	E
196	Surfeit locus protein 6	P70279	NA-binding	S
197	SWI/SNF complex 170 kDa subunit	Q8TAQ2	NA-binding	S
198	Sucrose non-fermenting protein 2 homologue	Q91ZW3	NA-binding	S
199	Synaptonemal complex protein 1	Q03410	NA-binding	S, E
200	Synaptonemal complex protein 2	Q9BX26	NA-binding	E
201	T-box transcription factor TBX3	O15119	NA-binding	S
202	Transcription elongation factor A protein 1	P23193	NA-binding	S
203	Transcription elongation regulator 1	O14776	NA-binding	E
204	Transcription factor LUZP	Q9ESV1	NA-binding	E
205	Tumor protein p73-like	Q9JJP6	NA-binding	S
206	Vascular actin single-stranded DNA-binding factor 2 p44 component	O35295	NA-binding	S
207	Vitamin D response element binding protein	Q9TTV2	NA-binding	S
208	Zinc finger protein 40	Q06054	NA-binding	E
209	Zinc finger protein 62 homologue	Q8NB50	NA-binding	E
210	Zinc finger protein 85	Q03923	NA-binding	S
211	Zinc finger protein 92	Q03936	NA-binding	S
212	Abnormal spindle-like microcephaly-associated protein	Q8IZT6	Nuclear	S, E
213	Brain-expressed X-linked protein 1	Q9R224	Nuclear	E
214	Cell proliferation antigen Ki-67, short form	P46013	Nuclear	E
215	Centrosomin B	P23116	Nuclear	E
216	Chmadrin	Q9XS53	Nuclear	S
217	Desmoyokin	Q09666	Nuclear	S
218	KARP-1-binding protein 1	Q91Y79	Nuclear	S
219	KRAB-zinc finger protein KID3	Q571J5	Nuclear	S

Continued overleaf

© 2008 The Authors
Journal compilation © 2008 by the Molecular Biology Society of Japan/Blackwell Publishing Ltd.

Table 1 *Continued*

	Name	Accession No.	Categories	Fraction
220	Lamin A/C	P02545	Nuclear	E
221	Matrin 3	P43243	Nuclear	E
222	Nesprin 1	Q8NF91	Nuclear	S
223	Rbm	Q60990	Nuclear	E
224	Uveal autoantigen	Q9BG87	Nuclear	S, E
225	Zinc finger protein DZIP1	Q8BMD2	Nuclear	E
226	Eukaryotic initiation factor 4A-I	P29562	Ribosomal	E
227	Eukaryotic initiation factor 4A-II	Q14240	Ribosomal	E
228	Eukaryotic translation initiation factor 2 subunit 1	P68101	Ribosomal	S
229	Eukaryotic translation initiation factor 2 subunit 2	Q99L45	Ribosomal	E
230	Eukaryotic translation initiation factor 3 subunit 10	Q14152	Ribosomal	E
231	Eukaryotic translation initiation factor 4-γ2	Q62448	Ribosomal	S
232	Ribosomal protein L3	P39023	Ribosomal	S
233	Ribosomal protein L35a	Q9DC85	Ribosomal	E
234	Ribosomal protein L4	Q9D8E6	Ribosomal	S
235	Ribosomal protein L7	P18124	Ribosomal	E
236	Ribosomal protein S11	P62280	Ribosomal	E
237	Ribosome-binding protein 1	Q9P2E9	Ribosome	S, E
238	Small nuclear ribonucleoprotein component U5	Q15029	Ribosomal	S
239	Adaptor-related protein complex AP-4 σ4 subunit	Q9Y587	Vesicle	S
240	Charged multivesicular body protein 2b	Q9UQN3	Vesicle	S
241	Clathrin heavy chain	P49951	Vesicle	S, E
242	Clathrin light chain B	P08082	Vesicle	E
243	Dynamin 1	P39053	Vesicle	S, E
244	Early endosome antigen 1	Q15075	Vesicle	S, E
245	ERC protein 2	Q8K3M6	Vesicle	E
246	Exocyst complex component 7	Q9UPT5	Vesicle	S
247	Flotillin-1	O75955	Vesicle	S
248	Kinectin	Q86UP2	Vesicle	E
249	Plasmalemma vesicle-associated protein	Q91VC4	Vesicle	S
250	PV1 (Plasmalemma vesicle-associated protein)	Q9BX97	Vesicle	S, E
251	Rab GDP dissociation inhibitor2	O97556	Vesicle	S
252	RAB11 family interacting protein 4	Q86YS3	Vesicle	E
253	Rab2, GTP-binding protein Rab2	P61019	Vesicle	S
254	Rab6-interacting protein 2	Q99MI1	Vesicle	S, E
255	Rabphilin-3A	P47708	Vesicle	E
256	RUN and FYVE domain-containing protein 2	Q8R4C2	Vesicle	S, E
257	SH3 domain protein 2A	Q62420	Vesicle	S
258	Soluble NSF attachment protein α	P54921	Vesicle	E
259	Soluble NSF attachment protein β	Q8N8N1	Vesicle	S, E
260	Soluble NSF attachment protein γ	Q99747	Vesicle	E
261	Synapsin IIa	Q63537	Vesicle	E
262	Synapsin IIb	Q92777	Vesicle	E
263	Synapsin-1	P09951	Vesicle	S
264	Synaptojanin 2	Q9D2G5	Vesicle	S
265	Synaptotagmin-like protein 3	Q99N48	Vesicle	S
266	Transitional endoplasmic reticulum ATPase	P46462	Vesicle	S
267	14-3-3 protein β/α	P31946	Diverse	E
268	14-3-3 protein η	P68510	Diverse	E
269	14-3-3 protein γ	P68252	Diverse	E
270	14-3-3 protein ζ/δ	P63102	Diverse	E
271	14-3-3 protein, ε	P62260	Diverse	E
272	14-3-3 protein, θ	P68255	Diverse	E
273	26S protease regulatory subunit 8	P62198	Diverse	E
274	26S proteasome non-ATPase regulatory subunit 12	Q9D8W5	Diverse	E
275	Activation-induced cytidine deaminase	Q8NFC4	Diverse	E
276	α-Internexin	P46660	Diverse	E
277	ARF GTPase-activating protein GIT1	Q9Z272	Diverse	S

Continued overleaf

© 2008 The Authors
Journal compilation © 2008 by the Molecular Biology Society of Japan/Blackwell Publishing Ltd.

Table 1 *Continued*

	Name	Accession No.	Categories	Fraction
278	Ca^{2+}/calmodulin-dependent protein kinase II β-chain	P08413	Diverse	S
279	cAMP-dependent protein kinase type II-α regulatory chain	Q8K1M3	Diverse	S
280	cAMP-dependent protein kinase type II-β regulatory subunit	P12369	Diverse	S
281	cAMP-dependent protein kinase, α-catalytic subunit	Q9MZD9	Diverse	S
282	cAMP-dependent protein kinase, β-catalytic subunit	P22694	Diverse	E
283	Carboxy terminus of HSP70-interacting protein	Q9UNE7	Diverse	S
284	Carnitine deficiency-associated protein expressed in ventricle 1	Q8WYA0	Diverse	E
285	Caskin-1	Q8VHK2	Diverse	E
286	Caspase-1	Q9TV13	Diverse	E
287	CENP-F kinetochore protein	P49454	Diverse	E
288	Citron ρ-interacting kinase	P49025	Diverse	S, E
289	Coiled-coil and C2 domain-containing protein 1A	Q8K1A6	Diverse	S
290	CUB and sushi multiple domains protein 2	Q7Z408	Diverse	S, E
291	Cullin-4B	Q13620	Diverse	S
292	Cytochrome *c* oxidase assembly protein COX19	Q8K0C8	Diverse	E
293	Cytochrome P450 2D6	P10635	Diverse	S
294	Dendrotoxin α-dendrotoxin-sensitive potassium channel β	Q27955	Diverse	E
295	Desmoplakin	P15924	Diverse	E
296	Diacylglycerol kinase γ	P49619	Diverse	S
297	Dihydrolipoyllysine-residue acetyltransferase component of pyruvate dehydrogenase complex	P08461	Diverse	S, E
298	Dual-specificity tyrosine-phosphorylation regulated kinase 2	Q92630	Diverse	S
299	DVL-binding protein DAPLE	Q6VGS5	Diverse	E
300	Filamin A interacting protein 1	Q7Z7B0	Diverse	E
301	Focal adhesion kinase 1	P34152	Diverse	S
302	Fructose-bisphosphate aldolase A	P05065	Diverse	S, E
303	Fructose-bisphosphate aldolase C	P09972	Diverse	S
304	G protein-coupled receptor-associated sorting protein 1	Q5U4C1	Diverse	E
305	Glutamine synthetase	P09606	Diverse	S
306	Glyceraldehyde-3-phosphate dehydrogenase	P04797	Diverse	S
307	Glycogen synthase kinase-3α	P49840	Diverse	S
308	Glycogen synthase kinase-3β	P18266	Diverse	S
309	Glycosyl-phosphatidyl-inositol-anchored protein p137-like	Q6YF16	Diverse	E
310	GRIN1	Q3UNH4	Diverse	E
311	Hexokinase 1	Q91W97	Diverse	E
312	Liprin α1	Q13136	Diverse	S
313	Liprin α4	Q91Z80	Diverse	S
314	Membrane-associated progesterone receptor component 1	O00264	Diverse	S
315	Mirror-image polydactyly gene 1 protein	Q8TD10	Diverse	S, E
316	Myotubularin-related protein 8	Q96EF0	Diverse	S
317	N2B-titin isoform	Q8WZ42	Diverse	S
318	Nasopharyngeal epithelium specific protein 1	Q9D9U9	Diverse	S
319	Nebulin-related anchoring protein	Q86VF7	Diverse	S
320	Osmosis responsive factor	Q6PID6	Diverse	S, E
321	Proliferation potential-related protein	Q7Z6E9	Diverse	S
322	Proteasome subunit α-type 1	P25786	Diverse	S, E
323	Proteasome subunit α-type 4	Q9R1P0	Diverse	S
324	Protein kinase C inhibitor KCIP-1 isoform δ	Q7M332	Diverse	S
325	Protein kinase C-α binding protein	Q9NRD5	Diverse	S
326	Protein phosphatase 2, α-isoform of regulatory subunit A	P30153	Diverse	S
327	Pyruvate dehydrogenase E1 component α-subunit	P08559	Diverse	S
328	Ras-GTPase-activating protein binding protein 2	P97379	Diverse	S, E
329	Receptor tyrosine kinase-like orphan receptor 2	Q9Z138	Diverse	S
330	Regulator of G protein signaling protein	Q86UV0	Diverse	S
331	ρ/rac guanine nucleotide exchange factor (GEF) 2	Q60875	Diverse	S
332	ρ-associated protein kinase 1	Q63644	Diverse	S, E
333	ρ-associated protein kinase 2	Q62868	Diverse	S, E

Continued overleaf

© 2008 The Authors
Journal compilation © 2008 by the Molecular Biology Society of Japan/Blackwell Publishing Ltd.

Table 1 *Continued*

	Name	Accession No.	Categories	Fraction
334	Ribosomal protein S6 kinase α5	O75582	Diverse	S
335	RING finger protein 20	Q5VTR2	Diverse	S
336	SAD1 kinase	Q8TDC3	Diverse	S
337	Serine/threonine kinase 10	Q62830	Diverse	E
338	SSX5 protein	O60225	Diverse	S
339	Staphylococcal nuclease domain containing 1	Q7KZF4	Diverse	E
340	STIP1 homology and U-Box containing protein 1	Q9WUD1	Diverse	S
341	Transcription elongation factor B polypeptide 3 binding protein 1	Q8N1G1	Diverse	S
342	Tripartile motif protein2	Q9ESN6	Diverse	S
343	Tripartile motif protein46	Q95J41	Diverse	S
344	tRNA pseudouridine synthase A	Q9WU56	Diverse	E
345	Testis-specific gene 10 protein	Q9BZW7	Diverse	S
346	Uaca protein	Q8CIA8	Diverse	S
347	Voltage-gated potassium channel β-2 subunit	P62482	Diverse	S
348	X-ray repair complementing defective repair in Chinese hamster cells 5	Q8C4N6	Diverse	S
349	Zinc finger FYVE domain containing protein 19	Q96K21	Diverse	S
350	BC004690 protein	Q99KF2	Uncharacterized	S
351	C6orf97 protein	Q8IYT3	Uncharacterized	E
352	CGI-62 protein	Q96GY0	Uncharacterized	S
353	Coiled-coil domain containing protein 13	Q8IYE1	Uncharacterized	S, E
354	Coiled-coil domain containing protein 9	Q8VC31	Uncharacterized	S
355	FLJ21438 protein	Q8N2T9	Uncharacterized	E
356	Hypothetical	Q68DY1	Uncharacterized	E
357	Hypothetical	Q9UFB7	Uncharacterized	E
358	Hypothetical	Q95JK1	Uncharacterized	E
359	Hypothetical	Q96DK7	Uncharacterized	E
360	Hypothetical	Q96LI9	Uncharacterized	E
361	Hypothetical	Q9H943	Uncharacterized	E
362	Hypothetical	Q8K303	Uncharacterized	E
363	Hypothetical	Q5T655	Uncharacterized	E
364	Hypothetical	Q95JL6	Uncharacterized	E
365	Hypothetical	Q9BE47	Uncharacterized	E
366	Hypothetical	Q9NXG0	Uncharacterized	E
367	Hypothetical	Q8N8E3	Uncharacterized	E
368	Hypothetical	Q9NWK9	Uncharacterized	E
369	Hypothetical	Q96LP2	Uncharacterized	E
370	LRRC40 (Leucine-rich repeat-containing protein 40)	Q9CRC8	Uncharacterized	S
371	Hypothetical	Q6NZL0	Uncharacterized	S
372	Hypothetical	Q95JX8	Uncharacterized	S
373	Hypothetical	Q96MC5	Uncharacterized	E
374	Hypothetical	Q9D4V3	Uncharacterized	E
375	Hypothetical protein DKFZp434C196	Q9UF83	Uncharacterized	S
376	Hypothetical protein DKFZp564J047	Q5T0J7	Uncharacterized	S
377	Hypothetical, GRINL1A combined protein isoform 7	Q96NF5	Uncharacterized	S
378	Hypothetical, RIKEN cDNA 1700001L19	Q9DAR0	Uncharacterized	E
379	KIAA0542 protein	O60289	Uncharacterized	S
380	KIAA0692 protein	Q86XL3	Uncharacterized	S
381	KIAA1505 protein	Q8IYE0	Uncharacterized	E
382	CCDC40/KIAA1640 protein	Q8BI79	Uncharacterized	S, E
383	KIAA1937 protein	Q96PV1	Uncharacterized	E
384	LRRC45 (Leucine-rich repeat-containing protein 45)	Q8CIM1	Uncharacterized	E
385	MAP7 domain-containing protein 1	A2AJI0	Uncharacterized	S
386	MAP7 domain-containing protein 2	Q96T17	Uncharacterized	S, E
387	Protein C10orf118	Q7Z3E2	Uncharacterized	E
388	Protein C14orf145	Q6ZU80	Uncharacterized	E
389	RIKEN cDNA 2010300C02	Q9D852	Uncharacterized	E
390	Spermatogenesis-associated serine-rich protein 2	Q86XZ4	Uncharacterized	S
391	Uncharacterized protein C2orf16	Q68DN1	Uncharacterized	S

E, extract fraction; NA, uncleic acid; S, soluble fraction.

© 2008 The Authors
Journal compilation © 2008 by the Molecular Biology Society of Japan/Blackwell Publishing Ltd.

Table 2 Characterization of six unknown proteins

Name	Accession No.	Size (amino acids)	Domain	Localization
FLJ21438	Q8N2T9	264	None	Vesicular
LRRC40	Q9CRC8	602	LRR	Cytoplasmic
Hypothetical	Q96MC5	204	None	Vesicular
KIAA1505	Q8IYE0	955	CC	Centrosomes
CCDC40/KAA1640	Q8BI79	1192	CC	Cilia
LRRC45	Q8CIM1	670	CC/LRR	Centrosomes

LRR, leucine-rich repeat domain; CC, coiled-coil domain.

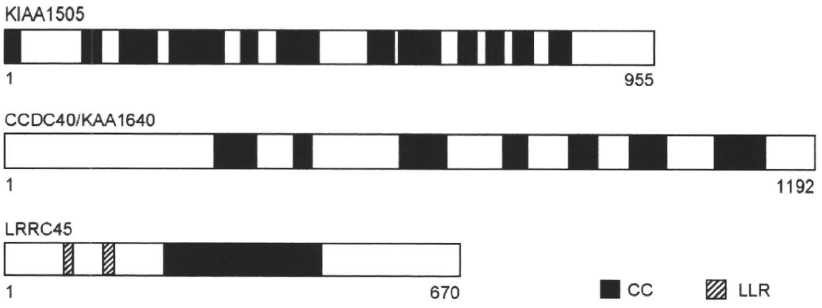

Figure 5 Structures of three uncharacterized proteins. CC, coiled-coil domain; and LRR, leucine-rich repeat domain.

co-localized with the centrosomal protein γ-tubulin (Figs 5 and 6). These results indicate that these two proteins are novel components of centrosomes.

CCDC40/KIAA1640 also contained coiled-coil domains (Fig. 5). This protein was co-localized with acetylated tubulin in RPE-1 cells (Fig. 6). Acetylated tubulin is known as a marker protein for detection of the primary cilia (Pipemo & Fuller 1985). To confirm the localization of CCDC40, this protein was expressed in MDCK cells grown on 7-day post-confluence. The staining pattern of CCDC40 was similar to that of acetylated tubulin (Fig. 7). Taken together, these results indicate that CCDC40 is a novel component of cilia.

Discussion

We analyzed MT co-sedimented proteins by MS/MS upon ion exchange column chromatography. The proteins identified were grouped into 12 different categories on the basis of functions and/or localization.

MT cytoskeletal proteins

Our analysis detected many MAPs previously shown to be biochemically associated with MTs. These included not only side-binding proteins (e.g. MAP1A/B, MAP2 and τ) but also plus-end-binding proteins (e.g. CLIP-115, CLIP-170 and EB1). However, we failed to identify several MAPs, such as MAP4, APC, NuMA and CENP-E. These MAPs may have been missed by MS because of an extremely low abundance in the brain or weak interaction with MTs (removed by washing). Furthermore, a minus-end-binding protein, γ-tubulin, was not identified. γ-Tubulin not only associates with centrosomes but also exists as a cytosolic form (Moudjou *et al.* 1996). The cytosolic form is shown to be capable of binding to taxol-stabilizing MTs. This binding of γ-tubulin to MTs is resistant to salt, ATP and GTP treatment. Thus, a possible explanation for the absence of γ-tubulin in our identified proteins is that γ-tubulin was co-sedimented with MTs but was not released from MTs with NaCl and ATP.

Other cytoskeletal proteins

We detected actin, intermediate filaments and septin cytoskeletal proteins. MTs, actin microfilaments and intermediate filaments are the three main cytoskeletal systems (Rodriguez *et al.* 2003; Chang & Goldman 2004). Although these systems are composed of distinctly different proteins, they are assumed to interact with each other. Septins are also regarded as cytoskeletal components that associate with the actin and MT cytoskeleton (Spiliotis & Nelson 2006). We identified several molecular linkers for mediating structural interactions of these cytoskeletal systems. MAP2 possesses both actin- and MT-binding sites and is regarded as a linker protein

© 2008 The Authors
Journal compilation © 2008 by the Molecular Biology Society of Japan/Blackwell Publishing Ltd.

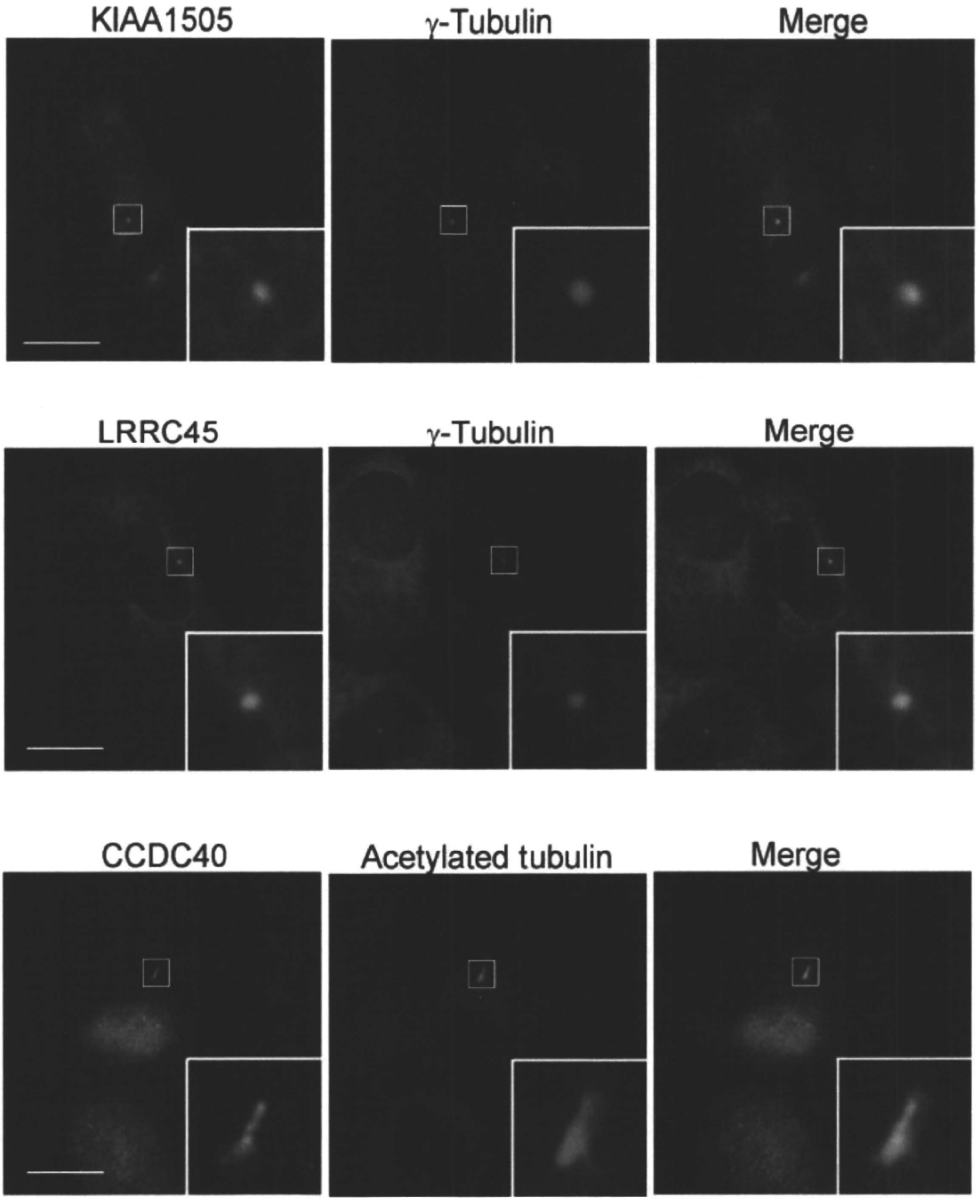

Figure 6 Localization of three uncharacterized proteins. EGFP-fusion proteins of KIAA1505, LRRC45 and CCDC40 were transiently expressed in RPE-1 cells. Cells were double stained with anti-EGFP Ab and anti-γ-tubulin Ab or anti-acetylated tubulin Ab. Samples were examined with a fluorescence microscopy. There was cytoplasmic or nuclear staining, but its significance is not clear. Insets, enlarged images of boxes. Scale bars, 10 μm.

between actin and MTs (Rodriguez *et al.* 2003). Intermediate filaments are assumed to be critical in mediating structural interactions between MTs and actin, functioning through plakins, a family of cytoskeletal cross-linkers. Plakins are large multidomain proteins that bind intermediate filaments and are essential for maintaining tissue integrity (Chang & Goldman 2004). Several plakins, including plectin, bullous pemphigoid antigen 1 and

© 2008 The Authors
Journal compilation © 2008 by the Molecular Biology Society of Japan/Blackwell Publishing Ltd.

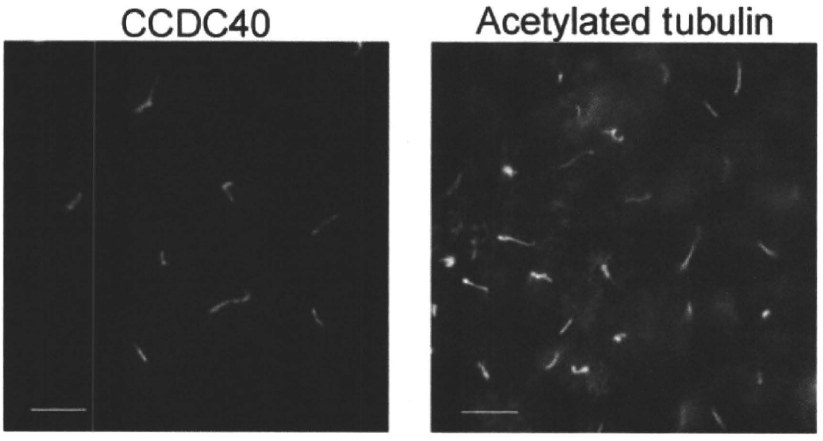

Figure 7 Localization of CCDC40 at cilia. MDCK cells were transfected with a recombinant retrovirus carrying Myc-tagged CCDC40. MDCK cells were grown for 7 days on Transwell filters. Cells were single stained with anti-Myc Ab or anti-acetylated tubulin Ab. The samples were examined with a fluorescence microscopy. Scale bars, 10 μm.

MT-actin cross-linking factor, also contain actin- and MT-binding sites. Identification of MAP2 and plakins, together with the actin and intermediate filament proteins, suggests that the three cytoskeletal systems are interlinked by these linker proteins.

Centrosomal proteins

chTOG, which we identified, is an MAP predominantly localized at centrosomes (Kinoshita *et al.* 2002), although this protein was classified here into MT cytoskeletal proteins. Identification of this MAP indicates that our method is useful for detecting low abundant MAPs localized at MT-based structures. Several other components of centrosomes were also identified. It is not clear how they were co-sedimented with MTs, but chTOG is known to interact with centrosomal proteins (Ohkura *et al.* 2001). chTOG may mediate interaction of these centrosomal proteins with MTs.

Chaperones

We identified several chaperones. HSP70s were originally characterized as MAPs before they were identified as molecular chaperons (Liang & MacRae 1997). HSP90 was also shown to associate with MTs in cultured cells. Furthermore, it was shown that the chaperons directly associate with τ, an MAP, and increase the association of τ with MTs (Dou *et al.* 2003). On the basis of these observations, it is proposed that molecular chaperones have roles in MT organization (Liang & MacRae 1997). Our results are consistent with this proposal.

Other proteins

MTs not only play a role in sister chromatid segregation, but also serve as major tracks for the intracellular transport of ribosomes, mitochondria, membrane vesicles and RNA granules. RNA granules transport a subset of mRNAs to axons or dendrites through RNA-binding proteins, referred to as heterogeneous nuclear ribonucleoproteins (hnRNPs), along MTs (Carson & Barbarese 2005; Anderson & Kedersha 2006). MTs are furthermore involved in the migration and positioning of the nucleus and Golgi, although it is poorly understood how the nucleus and Golgi interact with MTs (Barr & Egerer 2005; Starr 2007). Several proteins localized at these organelles were consistently identified, suggesting that these proteins may directly or indirectly interact with MTs. In addition, we identified many proteins with diverse cellular functions and/or localization. Similar multiplicity has also been reported in MS screening of MT-based structures, spindles and cilia (Ostrowski *et al.* 2002; Sauer *et al.* 2005). Consistent with these previous reports, our results suggest that many more proteins are involved in MT-based functions and structures than previously assumed.

A major concern is nonspecific contamination by proteins unrelated to MTs. Such contamination would contribute artifactually to the observed multiplicity of MT co-sedimented proteins. However, we identified hnRNP A2, a component of RNA granules, which is shown to bind to chTOG and proposed to mediate the association of hnRNP A2-positive granules with MTs (Kosturko *et al.* 2005). Furthermore, KARP-1-binding protein 2/KAB1/Cep170 was originally identified as a binding partner of KARP-1, a DNA-binding protein (Do *et al.* 2003), but it has been found to associate with the mature mother centrioles and spindle MTs during mitosis (Guarguaglini *et al.* 2005). It is, therefore, plausible that at least some of presumptive impurities actually reflect a specific association with MTs or a role as MAPs.

Of 42 uncharacterized proteins, three proteins with coiled-coil domains (KIAA1505, LRRC45 and CCDC40) were novel components of centrosomes and cilia. In

© 2008 The Authors
Journal compilation © 2008 by the Molecular Biology Society of Japan/Blackwell Publishing Ltd.

addition, we have found another novel centrosomal protein (Q9NXG0) and named it centlein (Makino *et al.* 2008). This protein also contains coiled-coil domains. Centrosomes are known to be made up of numerous proteins with coiled-coil domains (Doxsey *et al.* 2005). Increasing evidence indicates that this molecular structure may be well designed for the organization of protein complexes, such as MT-based structures. Of the uncharacterized proteins, those with coiled-coil domains are highly expected to be components of MT-based structures.

Compared to previous MS analyses of isolated MT-based structures, such as centrosomes, cilia and mitotic spindles (Ostrowski *et al.* 2002; Andersen *et al.* 2003; Keller *et al.* 2005; Pazour *et al.* 2005; Sauer *et al.* 2005; Nousiainen *et al.* 2006; Reinders *et al.* 2006), our method is characterized by anion exchange column chromatography used to enrich low abundant proteins. It is likely that this chromatography contributes to the identification of novel components of centrosomes and cilia, which have not been previously identified. In conclusion, our present method is useful for identifying low abundant novel MAPs and components of MT-based structures. Our analysis provides an extensive list of potential candidates for future analysis. It is important to follow up the proteomics approach with more focused experiments to examine whether these candidate proteins show a specific association with MTs and/or MT-based structures and, if so, what their physiological functions are?

Experimental procedures

Preparation of MTs

Tubulin was purified from fresh porcine brains by three cycles of polymerization and depolymerizaiton (Shelanski *et al.* 1973) followed by DEAE-Sephadex column chromatography (Williams & Lee 1982). Purified tubulin was stored at −80 °C until use. MTs were prepared by incubation of purified tubulin (4 mg/mL) for 20 min at 37 °C in polymerization buffer (80 mM PIPES–NaOH, pH 6.8, 1 mM $MgCl_2$, 1 mM EGTA, 1 mM GTP and 10% glycerol) (Yamamoto *et al.* 2002; Uezu *et al.* 2007). After the incubation, taxol was added to give a final concentration of 15 μM.

Preparation and resolution of MT co-sedimented proteins

All the purification procedures were carried out at 0–4 °C. Twenty rat brains were homogenized in 100 mL of buffer A (50 mM HEPES–NaOH, pH 7.5, 5 mM EGTA, 2 mM EDTA, 1 mM DTT, 50 mM NaF, 1 mM Na_3VO_4, 0.1% Triton X-100, 1 mM PMSF, 10 μg/mL of leupeptin and 1 μg/mL of pepstatin A). The homogenate was subjected to ultracentrifugation at 100 000 ***g*** for 1 h. The supernatant and pellet were employed as the soluble and insoluble fractions, respectively. MT co-sedimented proteins from the soluble fraction were prepared as follows: $MgCl_2$, GTP and taxol were added to the soluble fraction to give final concentrations of 4 mM, 1 mM and 20 μM, respectively. The sample was then incubated with 1 mg/mL of MTs for 3 h. The mixture was placed over a 20-mL cushion of 10% sucrose in HEM buffer (50 mM HEPES–NaOH, pH 7.5, 1 mM EGTA, 1 mM $MgCl_2$, 50 mM NaF, and 1 mM Na_3VO_4, 1 mM GTP and 20 μM taxol), followed by ultracentrifugation at 100 000 ***g*** for 30 min. The pellet (P1) was rinsed with HEM buffer and then homogenized in 20 mL of HEM buffer containing 50 mM NaCl, followed by ultracentrifugation at 100 000 ***g*** for 30 min. The pellet (P2) was rinsed with HEM buffer and then homogenized in 20 mL of HEM buffer containing 0.5 M NaCl and 0.1 mM ATP to dissociate co-sedimented proteins from MTs, followed by ultracentrifugation at 100 000 ***g*** for 30 min. The supernatant (S3, 24 mg of protein) was collected and used as MT co-sedimented proteins from the soluble fraction.

The extract fraction was prepared as follows: the insoluble fraction was re-homogenized in 20 mL of buffer A containing 1.0 M NaCl. The homogenate was mildly stirred for 30 min and centrifuged at 100 000 ***g*** for 1 h. The supernatant was diluted with 120 mL of buffer A, followed by ultracentrifugation at 100 000 ***g*** for 1 h. The supernatant was collected and the concentration of NaCl was examined by measuring the conductivity. The sample was further diluted with buffer A and brought to a final concentration of 100 mM NaCl. This sample was employed as the extract fraction. The extract fraction was then subjected to MT co-sedimentation in the same manner as described above.

MT co-sedimented proteins from the soluble and extract fractions (10 mg of protein each) were separately subjected to precipitation by a chloroform–methanol–water system (Pohl 1990) and dissolved in 5 mL of buffer B (40 mM Tris–HCl, pH 8.0, 1 mM EDTA, 1 mM DTT, 0.6% CHAPS and 4 M urea). The sample was applied to a BioAssist Q column (4.6 × 50 mm; Tosoh, Tokyo, Japan) equilibrated with buffer B. The column was washed with 20 mL of buffer B, and elution was performed with a 12.5-mL linear gradient (0–0.25 M) of NaCl in buffer B and a subsequent 6.25-mL linear gradient (0.25–0.5 M) of NaCl in buffer B, followed by 6.25 mL of 1 M NaCl in buffer B. Fractions of 0.5 mL each were collected.

Identification by MS/MS analysis

Each fraction of BioAssist Q column chromatography was subjected to SDS-PAGE (10% polyacrylamide gel), followed by protein staining with silver (Shevchenko *et al.* 1996). Each protein band was excised and digested with trypsin (Promega, Madison, WI). After destaining with 100 μL of 10 mM potassium ferricyanide and 50 mM sodium thiosulfate (Gharahdaghi *et al.* 1999), the gel pieces were dried and swollen in digestion buffer [50 mM ammonium bicarbonate, 10% acetonitrile (ACN) and 10 ng/μL trypsin], and incubated at 37 °C for 16 h. Peptides were extracted by 30% and 80% ACN then concentrated in a vacuum centrifuge. Dried samples were dissolved in 15 μL of 0.1% trifluoroacetic acid (TFA) then desalted by Zip tips C18 (Millipore, Bedford, MA)

© 2008 The Authors
Journal compilation © 2008 by the Molecular Biology Society of Japan/Blackwell Publishing Ltd.

and peptides were mixed with matrix solution (10 mg/mL a-cyano-4-hydroxycinnamic acid in 50% ACN and 0.1% TFA) and crystallized onto the 576-well target plate. Matrix-laser desorption/ionization-time of flight (TOF) and tandem TOF data were acquired in batch mode using an ABI4700 Proteomics Analyzer (Applied Biosystems. Foster City, CA). MS reflector positive ion mode with automated acquisition of 800–4000 m/z range was used with 1000 shots per spectrum. A maximum of 10 peaks were selected per spot, with a minimum signal : noise ratio of 10 and a cluster area of 200. Precursor ions were submitted for MS/MS, where a positive ion mode with a collision induced-dissociation cell and 1kV collision energy were used, and 5000 shots were accumulated per spectrum. Database searching was performed with the GPS EXPLORER SOFTWARE (Applied Biosystems) utilizing Mascot (v1.9) at the search engine (Matrix Science Ltd., London, UK) allowing ±0.3 Da as the parent tolerance and ±0.1 Da as the fragment ion tolerance. Combined peak lists were searched against the non-redundant Swiss-Prot database, and the oxidation of methionine and one possible missed cleave site was selected as a variable modification. Peptides were considered identified if their Mascot score was at or over the 95% confidence limit; meaning that the fragmentation data is of sufficient quality as to have a > 95% probability of being assigned to the proper peptide sequence. Proteins were considered identified if at least one peptide matched to it with a significant Mascot score.

Molecular cloning

Q8N2T9 was obtained from the Kazusa DNA Research Institute. Q8IYE0 was purchased from Invitrogen (Carlsbad, CA) (MGC clone, 5273288). Q8BI79 (RikenB930008102) was purchased from DNAFORM (Yokohama, Japan). The following cDNAs were obtained by PCR : Q9CRC8, (primers) 5′-CTG CAG CTT CTG GAC CTA GGA CTT TG-3′ and 5′-ATG ACA AGG GTT ATA AAG CAA CTC CAT G-3′, (template) HeLa cell cDNA; Q96MC5, (primers) 5′-GAT CAG CGA TGG AAT TAA AGC AAT C-3′ and 5′-GAC TCC CTA CTG CTA CAC TCT GTA CAG-3′, (template) HeLa cell cDNA; and Q8CIM1, (primers) 5′-GAA TTC ATG GAG GAG TTC CGG CGC TCC TAC-3′ and 5′-GTC GAC TCA TTT AGG GGG ATC CAA GGC TCT C-3′, (template) mouse brain cDNA. These cDNAs were cloned into pEGFP-C1 (Clontech. Mountain View, CA) and pMXII-Myc (Ono *et al.* 2000).

Cell culture, transfection and immunofluorescence microscopy

RPE-1 and MDCK cells were maintained at 37 °C in Dulbecco's modified Eagle's medium supplemented with 10% fetal calf serum. Transfection was performed using FuGene6 (Roche Diagnostics, Basel, Switzerland) transfection reagent according to the manufacturer's protocol. For cilia immunostaining in RPE-1 cells, cells were cultured in medium with 0.25% serum for 48 h (Gromley *et al.* 2003). For cilia immunostaining in MDCK cells, a recombinant retrovirus carrying Myc-CDCC40 cDNA was prepared with pMXII-Myc (Nishimura *et al.* 2002). MDCK cells were infected with the recombinant retrovirus and cultured for 1 day. After the medium was changed, the cells were grown for 7 days post-confluence on 10 mm Transwell filters as described (Fan *et al.* 2004).

The following antibodies (Abs) were purchased from commercial sources: mouse anti-Myc monoclonal Ab (9E10) (American Type Culture Collection, Manassas, VA); mouse anti-acetylated tubulin (clone 6-11B-1) and mouse anti-γ-tubulin monoclonal Abs (Sigma-Aldrich, Seelze, Germany); rabbit anti-EGFP polyclonal Ab (MBL Co., Nagoya, Japan); and secondary Abs conjugated with Alexa Fluor 488 and 594 (Invitrogen). For immunofluorescence microscopy, cells were fixed in 100% methanol at –20 °C for 5 min. After blocking with 1% bovine serum albumin for 1 h at room temperature, the samples were incubated with primary Abs for 1 h, followed by incubation with second Abs for 30 min. The samples were viewed with a florescence microscope (Olympus, BX51).

Other procedures

Protein concentrations were determined with bovine serum albumin as a reference protein (Bradford 1976). SDS-PAGE was done as described (Laemmli 1970).

Acknowledgements

This study was supported by grants-in-aids for Scientific Research on Priority Areas from the Ministry of Education, Culture, Sports, Science, and Technology of Japan.

References

Andersen, J.S., Wilkinson, C.J., Mayor, T., Mortensen, P., Nigg, E.A. & Mann, M. (2003) Proteomic characterization of the human centrosomes by protein correlation profiling. *Nature* **426**, 570–574.

Anderson, P. & Kedersha, N. (2006) RNA granule. *J. Cell Biol.* **172**, 803–808.

Barr, F.A. & Egerer, J. (2005) Golgi positioning: are we looking at the right MAP? *J. Cell Biol.* **168**, 993–998.

Bettencourt-Dias, M. & Glover, D.M. (2007) Centrosome biogenesis and function: centrosomics brings new understanding. *Nat. Rev. Mol. Cell Biol.* **8**, 451–463.

Bradford, M.M. (1976) A rapid and sensitive method for the quantitation of microgram quantities of protein utilizing the principle of protein-dye binding. *Anal. Biochem.* **72**, 248–254.

Carson, J.H. & Barbarese, E. (2005) Systems analysis of RNA trafficking in neural cells. *Biol. Cell* **97**, 51–62.

Cassimeris, L. & Spittle, C. (2001) Regulation of microtubule-associated proteins. *Int. Rev. Cytol.* **210**, 163–226.

Chang, L. & Goldman, R.D. (2004) Intermediate filaments mediate cytoskeletal crosstalk. *Nat Rev. Mol. Cell Biol.* **5**, 601–613.

Do, E., Taira, E., Irie, Y., Gan, Y., Tanaka, H., Kuo, C.H. & Miki, N. (2003) Molecular cloning and characterization of rKAB1, which interacts with KARP-1, localizes in the nucleus and protects cells against oxidative death. *Mol. Cell. Biochem.* **248**, 77–83.

© 2008 The Authors
Journal compilation © 2008 by the Molecular Biology Society of Japan/Blackwell Publishing Ltd.

Dou, F., Netzer W.J., Tanemura, K., Li, F., Hartl, F.U., Takashima, A., Gouras, G.K., Greengard, P. & Xu, H. (2003) Chaperones increase association of τ protein with microtubules. *Proc. Natl. Acad. Sci. USA* **100**, 721–726.

Doxsey, S., McCollum, D. & Theurkauf, W. (2005) Centrosomes in cellular regulation. Annu. *Rev. Cell Dev. Biol.* **21**, 411–434.

Fan, S., Hurd, T.W., Liu, C-J., Straight, S.W., Weimbs, T., Hurd, E.A., Domino, S.E. & Margolis, B. (2004) Polarity proteins control ciliogenesis via kinesin motor interactions. *Curr. Biol.* **14**, 1451–1461.

Gharahdaghi, F., Weinberg, C.R., Meagher, D.A., Imai, B.S. & Mische, S.M. (1999) Mass spectrometric identification of proteins from silver-stained polyacrylamide gel: a method for the removal of silver ions to enhance sensitivity. *Electrophoresis* **20**, 601–605.

Gromley, A., Jurczyk, A., Sillibourne, J., Halilovic, E., Mogensen, M., Groisman, I., Blomberg, M. & Doxsey, S. (2003) A novel human protein of the maternal centriole is required for the final stages of cytokinesis and entry into S phase. *J. Cell Biol.* **161**, 535–545.

Guarguaglini, G., Duncan, P.I., Stierhof, Y.D., Holmström, T., Duensing, S. & Nigg, E.A. (2005) The forkhead-associated domain protein Cep170 interacts with Polo-like kinase 1 and serves as a marker for mature centrioles. *Mol. Biol. Cell* **16**, 1095–1107.

Keller, L.C., Romijn, E.P., Zamora, I., Yates, J.R. 3rd & Marshall, W.F. (2005) Proteomic analysis of isolated chlamydomonas centrioles reveals orthologs of ciliary-disease genes. *Curr. Biol.* **15**, 1090–1098.

Kellogg, D.R., Field, C.M. & Alberts, B.M. (1989) Identification of microtubule-associated proteins in the centrosome, spindle, and kinetochore of the early *Drosophila* embryo. *J. Cell Biol.* **109**, 2977–2991.

Kinoshita, K., Habermann, B. & Hyman, A.A. (2002) XMAP215: a key component of the dynamic microtubule cytoskeleton. *Trends Cell Biol.* **12**, 267–273.

Kirschner, M. & Mitchison, T. (1986) Beyond self-assembly: from microtubules to morphognesis. *Cell* **45**, 329–342.

Kosturko, L.D., Maggipinto, M.J., D'Sa, C., Carson, J.H. & Barbarese, E. (2005) The microtubule-associated protein tumor overexpressed gene binds to the RNA trafficking protein heterogeneous nuclear ribonucleoprotein A2. *Mol. Biol. Cell* **16**, 1938–1947.

Laemmli, U.K. (1970) Cleavage of structural proteins during the assembly of the head of bacteriophage T4. *Nature* **227**, 680–685.

Liang, P. & MacRae, T.H. (1997) Molecular chaperones and the cytoskeleton. *J. Cell Sci.* **110**, 1431–1440.

Linck, R.W. & Stephens, R.E. (2007) Functional protofilament numbering of ciliary, flagellar, and centriolar microtubules. *Cell Motil. Cytoskeleton* **64**, 489–495.

Makino, K., Umeda, K., Uezu, A, Hiragami, Y., Sakamoto, T., Ihn, H. & Nakanishi, H. (2008) Identification and characterization of the novel centrosomal protein centlein. *Biochem. Biophys. Res. Commun.* **366**, 958–962.

Moudjou, M., Bordes, N., Paintrand, M. & Bournes, M. (1996) γ-Tubulin in mammalian cells: the centrosomal and cytosolic forms. *J. Cell Sci.* **109**, 875–887.

Nishimura, M., Kakizaki, M., Ono, Y., Morimoto, K., Takeuchi, M., Inoue, Y., Imai, T. & Takai, Y. (2002) JEAP, a novel component of tight junctions in exocrine cells. *J. Biol. Chem.* **227**, 5583–5587.

Nousiainen, M., Silljé, H.H., Sauer, G., Nigg, E.A. & Körner, R. (2006) Phosphoproteome analysis of the human mitotic spindle. *Proc. Natl. Acad. Sci. USA* **103**, 5391–5396.

Ohkura, H., Carcia, M.A. & Toda, T. (2001) Dis1/TOG universal microtubule adaptors-one MAP for all. *J. Cell Sci.* **114**, 3805–3812.

Olmstead, J.B. (1986) Microtubule-associated proteins. *Ann. Rev. Cell Biol.* **2**, 421–457.

Ono, Y., Nakanishi, H., Nishimura, M., Kakizaki, M., Takahashi, K., Miyahara, M., Satoh-Horikawa, K., Mandai, K. & Takai, Y. (2000) Two actions of frabin: direct activation of Cdc42 and indirect activation of Rac. *Oncogene* **19**, 3050–3058.

Ostrowski, L.E., Blackburn, K., Radde, K.M., Moyer, M.B., Schlatzer, D.M., Moseley, A. & Boucher, R.C. (2002) A proteomic analysis of human cilia: identification of novel components. *Mol. Cell. Proteomics* **1**, 451–465.

Pazour, G.J., Agrin, N., Leszyk, J. & Witman, G.B. (2005) Proteomic analysis of a eukaryotic cilium. *J. Cell Biol.* **170**, 103–113.

Pipemo, G. & Fuller, M.T. (1985) Monoclonal antibodies specific for an acetylated form of α-tubulin recognize the antigen in cilia and flagella from a variety of organisms. *J. Cell Biol.* **101**, 2085–2094.

Pohl, T. (1990) Concentration of proteins and removal of solutes. *Methods Enzymol.* **182**, 68–83.

Reinders, Y., Schulz, I., Gräf, R. & Sickmann, A. (2006) Identification of novel centrosomal proteins in *Dictyostelium discoideum* by comparative proteomic approaches. *J. Proteome Res.* **5**, 589–598.

Richard, J.E. & Kreis, T.E. (1990) Identification of a novel nucleotide-sensitive microtubule-binding protein in HeLa cells. *J. Cell Biol.* **110**, 1623–1633.

Rodriguez, O.C., Schaefer, A.W., Mandato, C.A., Forscher, P., Bement, W.M. & Waterman-Storer, C.M. (2003) Conserved microtubule–actin interactions in cell movement and morphogenesis. *Nat. Cell Biol.* **7**, 599–609.

Rogers, S.L. & Gelfand, V.I. (2000) Membrane trafficking, organelle transport, and the cytoskeleton. *Curr. Opin. Cell Biol.* **12**, 57–62.

Satir, P. & Christensen, S.T. (2007) Overview of structure and function of mammalian cilia. *Annu. Rev. Physiol.* **69**, 377–400.

Sauer, G., Körner, R., Hanisch, A., Ries, A., Nigg, E.A. & Silljé, H.H. (2005) Proteome analysis of the human spindle. *Mol. Cell. Proteomics* **4**, 35–43.

Shelanski, M.L., Gaskin, F. & Cantor, C.R. (1973) Microtubule assembly in the absence of added nucleotides. *Proc. Natl. Acad. Sci. USA* **70**, 765–768.

Shevchenko, A., Wilm, M., Vorm, O. & Mann, M. (1996) Mass spectrometric sequencing of proteins from silver-stained polyacrylamide gels. *Anal. Chem.* **68**, 850–858.

© 2008 The Authors
Journal compilation © 2008 by the Molecular Biology Society of Japan/Blackwell Publishing Ltd.

Siegrist, S.E. & Doe, C.Q. (2007) Microtubule-induced cortical cell polarity. *Genes Dev.* **21**, 483–496.

Spiliotis, E.T. & Nelson, W.J. (2006) Here comes the septins: novel polymers that coordinate intracellular functions and organization. *J. Cell Sci.* **119**, 4–10.

Starr, D.A. (2007) Communication between the cytoskeleton and the nuclear envelope to position the nucleus. *Mol. Biosys.* **3**, 583–589.

Uezu, A., Horiuchi, A., Kanda, K., Kikuchi, N., Umeda, K., Tsujita, K., Suetsugu, S., Araki, N., Yamamoto, H., Takenawa, T. & Nakanishi, H. (2007) SGIP1a is an endocytic protein that directly interacts with phospholipids and Eps15. *J. Biol. Chem.* **282**, 26481–26489.

Vallee, R.B., Bloom, G.S. & Theurkauf, W.E. (1984) Microtubule-associated proteins: subunits of the cytomatrix. *J. Cell Biol.* **99**, 38s–44s.

Wemmer, K.A. & Marshall, W.F. (2004) Flagella motility: all put together. *Curr. Biol.* **14**, R992–R993.

Williams, R.C. Jr. & Lee, J.C. (1982) Preparation of tubulin from brain. *Methods Enzymol.* **85**, 376–385.

Yamamoto, H., Yamauchi, E., Taniguchi, H., Ono, T. & Miyamoto, E. (2002) Phosphorylation of microtubule-associated protein τ by Ca2/calmodulin-dependent protein kinase II in its tubulin binding sites. *Arch. Biochem. Biophys.* **408**, 255–262.

Received: 20 November 2007
Accepted: 19 December 2007

© 2008 The Authors
Journal compilation © 2008 by the Molecular Biology Society of Japan/Blackwell Publishing Ltd.

Supplemental Material can be found at:
http://www.jbc.org/cgi/content/full/M708206200/DC1

THE JOURNAL OF BIOLOGICAL CHEMISTRY VOL. 283, NO. 14, pp. 9399–9413, April 4, 2008
© 2008 by The American Society for Biochemistry and Molecular Biology, Inc. Printed in the U.S.A.

Neurofibromatosis Type 1 (NF1) Tumor Suppressor, Neurofibromin, Regulates the Neuronal Differentiation of PC12 Cells via Its Associating Protein, CRMP-2*[S]

Received for publication, October 3, 2007, and in revised form, December 31, 2007 Published, JBC Papers in Press, January 23, 2008, DOI 10.1074/jbc.M708206200

Siriporn Patrakitkomjorn[‡], Daiki Kobayashi[‡], Takashi Morikawa[‡], Masayo Morifuji Wilson[‡], Nobuyuki Tsubota[‡], Atsushi Irie[§], Tatsuya Ozawa[‡], Masashi Aoki[‡], Nariko Arimura[¶], Kozo Kaibuchi[¶], Hideyuki Saya[‡], and Norie Araki[‡1]

From the [‡]Department of Tumor Genetics and Biology and [§]Department of Immunogenetics, Graduate School of Medical Sciences, Kumamoto University School of Medicine, Kumamoto 860-8556, and the [¶]Department of Cell Pharmacology, Nagoya University, Graduate School of Medicine, Nagoya, Aichi 466-8550, Japan

Neurofibromatosis type 1 (NF1) tumor suppressor gene product, neurofibromin, functions in part as a Ras-GAP, a negative regulator of Ras. Neurofibromin is implicated in the neuronal abnormality of NF1 patients; however, the precise cellular function of neurofibromin has yet to be clarified. Using proteomic strategies, we identified a set of neurofibromin-associating cellular proteins, including axon regulator CRMP-2 (Collapsin response mediator protein-2). CRMP-2 directly bound to the C-terminal domain of neurofibromin, and this association was regulated by the manner of CRMP-2 phosphorylation. In nerve growth factor-stimulated PC12 cells, neurofibromin and CRMP-2 co-localized particularly on the distal tips and branches of extended neurites. Suppression of neurofibromin using NF1 small interfering RNA significantly inhibited this neurite outgrowth and up-regulated a series of CRMP-2 phosphorylations by kinases identified as CDK5, GSK-3b, and Rho kinase. Overexpression of the NF1-RAS-GAP-related domain rescued these NF1 small interfering RNA-induced events. Our results suggest that neurofibromin regulates neuronal differentiation by performing one or more complementary roles. First, neurofibromin directly regulates CRMP-2 phosphorylation accessibility through the complex formation. Also, neurofibromin appears to indirectly regulate CRMP-2 activity by suppressing CRMP-2-phosphorylating kinase cascades via its Ras-GAP function. Our study demonstrates that the functional association of neurofibromin and CRMP-2 is essential for neuronal cell differentiation and that lack of expression or abnormal regulation of neurofibromin can result in impaired function of neuronal cells, which is likely a factor in NF1-related pathogenesis.

Neurofibromatosis type 1 (NF1)[2] is an autosomal dominantly inherited disorder, with an estimated prevalence of 1 in 3,000–4,000 people (1). The hallmarks of NF1 include development of benign tumors of the peripheral nervous system and an increased risk of developing malignancies. The phenotype of NF1 is highly variable, with several organ systems being affected, including the bones, skin, irises, and central and peripheral nervous systems. The effects on the nervous system manifest as neurofibroma, gliomas, and learning disabilities.

The *NF1* gene locates on chromosome 17q11.2 and encodes a large protein of 2,818 amino acids, neurofibromin (2). Because the great majority of *NF1* gene mutations frequently found in NF1 patients prevents the expression of intact neurofibromin, functional disruption of neurofibromin is potentially relevant to the expression of some or all of the multiple abnormalities that occur in NF1 patients (3).

A region centered around 360 amino acid residues encoded by the *NF1* gene shows significant homology to the known catalytic domains of mammalian Ras GTPase-activating protein (p120 GAP). This region is also similar to yeast IRA1/2 proteins, which have been shown to interact with Ras and mediate hydrolysis of Ras-bound GTP to GDP, resulting in inactivation of Ras protein function. The GAP-related domain of the *NF1* gene product (NF1-GRD) also stimulates Ras GTPase and consequently inactivates Ras protein (4–6). In the region of NF1-GRD, two different isoforms (type I and type II possessing higher and lower GAP activity, respectively) formed by alternative splicing have been identified (6).

Recently, we demonstrated a novel role for neurofibromin on neuronal differentiation in conjunction with regulation of Ras activity via its GAP-related domain (GRD) in NGF-stimulated PC12 cells serving as a model for neuronal cells (6). In PC12 cells, time-dependent increases in the GAP activity of cellular

* This work was supported by grants from, Cancer Research (to N. A.), Kiban Research (to N. A.), Houga Research (to N. A.) from the Ministry of Education, Science, and Culture of Japan (to N. A.), and from the Centers of Excellence Project B of Kumamoto University for proteomic research and education (to N. A.), from the Ministry of Health and Welfare of Japan (to H. S.), and from Japan Society for the Promotion of Science Asia and Africa Science Platform Program (to S. P. and N. A.). The costs of publication of this article were defrayed in part by the payment of page charges. This article must therefore be hereby marked "*advertisement*" in accordance with 18 U.S.C. Section 1734 solely to indicate this fact.

[S] The on-line version of this article (available at http://www.jbc.org) contains supplemental Movies 1 and 2 and Figs. S1–S5.

[1] To whom correspondence should be addressed: Dept. of Tumor Genetics and Biology, Graduate School of Medical Sciences, Kumamoto University, Kumamoto 860-8556, Japan. Tel.: 81-96-373-5323; Fax: 81-96-373-5120; E-mail: nori@gpo.kumamoto-u.ac.jp.

[2] The abbreviations used are: NF1, neurofibromin type 1; CRMP-2, collapsin response mediator protein-2; DN, dominant negative; GAP, GTPase-activating protein; GRD, GAP-related domain; siRNA, small interfering RNA; NGF, nerve growth factor; GST, glutathione *S*-transferase; CTD, C-terminal domain; CHAPS, 3-[(3-cholamidopropyl)dimethylammonio]-1-propanesulfonic acid; DTT, dithiothreitol; PBS, phosphate-buffered saline; PVDF, polyvinylidene difluoride; DIGE, difference gel electrophoresis; MS, mass spectrometry; MALDI-TOF, matrix-assisted laser desorption ionization time-of-flight; LC, liquid chromatography; ESI, electrospray ionization; CSRD, cysteine/serine-rich domain; FITC, fluorescein isothiocyanate; RhoK, Rho kinase.

Downloaded from www.jbc.org at KUMAMOTO UNIV LIB on March 1, 2009

neurofibromin (NF1-GAP) were detected after NGF stimulation, and these increases correlated with down-regulation of Ras activity during neurite elongation. Interestingly, the NF1-GAP increases were because of induction of alternative splicing of NF1-GRD type 1, which was triggered by NGF-induced Ras activation. Dominant-negative (DN) forms of NF1-GRD type I significantly inhibited the neurite extension of PC12 cells via regulation of the Ras state. NF1-GRD-DN also reduced axonal and dendritic branching/extension of rat embryonic hippocampal neurons. These results demonstrated that mutual regulation of Ras and NF1-GAP is essential for normal neuronal differentiation. Thus, we speculated that abnormal regulation of NF1-GAP in neuronal cells may be implicated in NF1-related learning and memory disorder (6). Recent studies using *Nf1* gene-targeting animals have also supported our hypothesis. For example, *Drosophila* homozygotes with *Nf1*-null mutation showed significant decrements in olfactory learning performance (4); *Nf1* heterozygous mice displayed spatial learning disability (7, 8), and mice lacking the alternatively spliced exon 23a of *Nf1* exhibited specific learning impairment (8). Furthermore, abnormal Ras activity in *Nf1* knock-out mice can disrupt learning and memory, indicating that the functional modulation of Ras by neurofibromin is essential for learning and memory.

To determine the precise cellular function of neurofibromin, we recently developed an acute knockdown system for neurofibromin using NF1-siRNAs, and we studied its effects on motility in several types of cell lines (9). In the glioma and HeLa cells, *NF1* siRNA treatment resulted in characteristic morphological changes such as abnormal actin stress fiber formation and elevated phosphorylation levels of cofilin, a protein that regulates actin cytoskeletal reorganization by depolymerizing and severing actin filaments. The elevated cofilin phosphorylation in neurofibromin-depleted cells was induced by activation of the Rho-RhoK/ROCK-LIMK2-cofilin pathway. Based on such evidence, we concluded that neurofibromin plays a significant role in actin cytoskeletal reorganization and cell motility (9).

The above observations prompted us to postulate that neurofibromin plays a key role in regulating cytoskeletal organization during axon formation or neurite outgrowth in neuronal cells, and that functional regulation by unknown factors associated with neurofibromin could collaborate in orchestrating these phenomena. The search for NF1-associated proteins is therefore of particular interest because it may both lead to the identification of novel cellular components in Ras-related and/or other pathways, as well as further our understanding of the mechanism of NF1-related pathogenesis.

In this study we analyzed the neurofibromin-associating proteins that functionally relate to neuronal cell differentiation. Using the newly established quantitative differential proteomic method, iTRAQ, more than 50 proteins were identified, including several neuronal regulating proteins. Out of the above, we focused on CRMP-2, which is known as a key molecule for axon formation and guidance. First, we observed that cellular colocalization of CRMP-2 and neurofibromin occurred especially on the neurites in NGF-treated PC12 cells. Subsequently, by suppressing neurofibromin expression using NF1 siRNA, we were able to analyze the functional association of CRMP-2 and neurofibromin in relation to the neurite outgrowth of PC12 cells. We observed that NF1 siRNA treatment resulted in up-regulation of a series of CRMP-2 phosphorylations and a significant inhibition of the neurite extension of NGF-treated PC12 cells. We then examined the functional correlation between CRMP-2 phosphorylation and neurofibromin suppression by analyzing specific related kinases in PC12 cells using unique proteomic strategies such as two-dimensional-DIGE combined with phosphoprotein staining and Western blotting using specific antibodies. Here we demonstrate that the neurofibromin function for neurite outgrowth of PC12 cells may involve the regulation of CRMP-2 phosphorylation via the direct interaction/complex formation with CRMP-2, and via the regulation of cellular CRMP-2 phosphorylating kinase cascades. We also discuss the implications of a functional association between neurofibromin and CRMP-2 for neuronal regulation in relation to NF1 pathogenesis.

EXPERIMENTAL PROCEDURES

Preparation of Glutathione S-transferase (GST) Fusion Proteins, Plasmid Constructions, and Transfections—GST fusion domain proteins of human neurofibromin corresponding to sequences of residues 543–909, 1168–1530, and 2260–2818 of neurofibromin, which were designated cysteine/serine-rich domain (CSRD), GAP-related domain (GRD), and C-terminal domain (CTD), respectively, were produced in *Escherichia coli* under the isopropyl 1-thio-β-D-galactopyranoside induction system and affinity-purified as described previously (10). Mammalian expression plasmids for NF1-GRD types 1 (pcDNA3-FLAG-GRD1X) were prepared as described previously (6). Human GST-CRMP2 plasmid construction and purification of GST-CRMP2 protein were performed as described previously (11). The GFP-NF1-CTD fusion protein expression vector was constructed by ligating KpnI/BamHI fragments of pAcGFP-C1 vector (Clontech) and pGEX-2TH/NF1-CTD (10). The vector was transfected to PC12 cells using Lipofectamine 2000 (Invitrogen) according to manufacturer's recommendation.

Antibodies and Inhibitors—An antibody against the C terminus of neurofibromin (anti-GRP (D)) was purchased from Santa Cruz Biotechnology (Santa Cruz, CA). The anti-human CRMP-2 (C4G) mouse IgG was purchased from IBL (Gunma, Japan). Monoclonal anti-α-tubulin (clone DM1A) and anti-β-tubulin (clone D66) were purchased from Sigma. The specific antibodies for phosphorylated CRMP-2, phospho-Thr^{514}, and phospho-Thr^{555} were prepared as described previously (12), and phospho-Ser^{522} was kindly provided from Dr. Y. Goshima (Yokohama City University). Secondary antibodies linked to horseradish peroxidase and Cy5 were purchased from Amersham Biosciences. Alexa Fluor® 488 goat anti-mouse IgG and Alexa Fluor® 568 goat anti-rabbit IgG were purchased from Invitrogen. Rhodamine phalloidin was purchased from Molecular Probes. ROCK inhibitor (Y27632), Cdk inhibitor (purvalanol A and olomoucine), and GSK-3β inhibitor (LiCl) were purchased from Calbiochem.

Purification of Binding Proteins from Mouse Brain Cytosolic Fraction by GST-CTD Affinity Chromatography—Mouse brain cytosolic fraction was prepared in lysis buffer A (20 mM Tris-

Downloaded from www.jbc.org at KUMAMOTO UNIV LIB on March 1, 2009

HCl, pH 7.5, 1 mM EDTA, 5 mM $MgCl_2$, 150 mM NaCl, and 0.1% Nonidet P-40) containing 1% protease inhibitors (mixture for mammalian tissues, Sigma) and 1 mM DTT, sodium fluoride (2 mM), sodium orthovanadate (2 mM), and okadaic acid (1 μM) as described (10). GST-CTD fusion proteins immobilized on GSH-agarose were packed onto a column and equilibrated with buffer B (30 mM Tris-HCl, pH 7.5, 1 mM EDTA, 5 mM $MgCl_2$, and 1 mM DTT). Mouse brain cytosolic fraction was pre-cleared by passing through a GSH column and then loaded onto the GST-CTD column or GST column as a control. After washing the column with buffer A, the proteins bound to the column were eluted by the addition of buffer C (buffer A containing 0.5 M NaCl) and used for the proteomic analysis. Protein concentrations of eluted samples were determined using the BCA protein assay (Pierce) or Bradford assay (Bio-Rad).

Silver Staining—Gels were fixed in fixative (50% methanol and 12% acetic acid) in 0.02% formaldehyde for at least 1 h. Gels were washed in 50% ethanol three times for 20 min and pretreated for 1 min by sodium thiosulfate (0.8 mM). Gels were rinsed in distilled water three times for 20 s. Silver nitrate solution (0.2%) in 0.03% formaldehyde was used for impregnating for 20 min, following rinsing with distilled water two times for 20 s. Developing solution (0.7 M of sodium carbonate, 0.02% formaldehyde, and 16 μM of sodium thiosulfate) was used for developing. Gels were rinsed two times in distilled water for 2 min. Stopping solution (50% methanol and 12% acetic acid) was used for stopping the reaction, and gels were kept in 50% methanol.

iTRAQ Sample Preparation and Quantitative Analysis—The 200 μl of protein samples (100 μg) were precipitated with 6× volume of acetone and kept overnight at −80 °C. After centrifugation of the samples at 13,000 × *g* for 5 min, the precipitants were kept and dissolved in 200 μl of 50 mM NH_4HCO_3, 2 mM $CaCl_2$, and 10% AcCN; then 1 μg of trypsin (Promega) was added and incubated at 37 °C for 2 h. Another 1 μg of trypsin was added before incubating overnight, after which the samples were kept at −80 °C until analysis. Samples were labeled with iTRAQ tags as follows: 100 μg of duplicated protein trypsin peptide fractions eluted from the GST-CTD column were labeled with iTRAQ116 and iTRAQ117; 100 μg of duplicated fractions from GST column as controls were labeled with iTRAQ114 and -115. The labeled samples were then all mixed, desalted, and subjected to LC-ESI-QQ-TOF and LC-MALDI-TOF-TOF MS analysis using the UltiMate NanoLC system (LCPackings A Dionex Company), the API QSTAR Pulsar i, or the 4700 Proteomics analyzer (Applied Biosystems). Obtained data were processed with iTRAQ quantitative analysis software ProQuant version 1.1 for ESI-QQ-TOF MS or GPS Explorer version 3.1 for MALDI-TOF-TOF MS (Applied Biosystems) and MASCOT (Matrix Science).

Immunoprecipitation Assays—Mouse brain was homogenized with lysis buffer A containing 1% protease inhibitor mixture for mammalian tissues (Sigma) and 1 mM DTT, sodium fluoride (2 mM), sodium orthovanadate (2 mM), and okadaic acid (1 μM) as the phosphatase inhibitors. Samples were centrifuged at 10,000 rpm for 10 min, and the supernatants were mixed with the indicated antibodies for 3 h and then mixed with appropriate protein A or G-Sepharose 4 Fast Flow beads (GE Healthcare) for 1 h. The beads were washed with buffer A, and boiled in 2× SDS loading buffer. Samples were separated by SDS-PAGE, transferred into PVDF membrane electrophoretically, and subjected to immunoblotting analysis with the indicated antibodies. After reaction with horseradish peroxidase- or Cy5-conjugated secondary antibodies, the reacted protein pattern on the membrane was visualized by an ECL detection system or by scanning with fluorescent scanner Typhoon 9400 (GE Healthcare), respectively.

Binding Assay of CRMP-2 to Neurofibromin Fragments in Vitro—The GST fusion neurofibromin fragment proteins (GST-CSRD-(543–909), GST-GRD-(1168–1530), GST-CTD-(2260–2818)), or GST (500 μg) purified from *E. coli* were immobilized on GSH-agarose beads and packed onto columns. CRMP-2 protein (500 μg) was prepared after the thrombin (48 units) treatment of GST-CRMP-2 in thrombin cleavage buffer (50 mM Tris-HCl, pH 8.8, 150 mM NaCl, 2.5 mM $CaCl_2$) for 40 min at room temperature, followed by the gel filtration. Purified CRMP-2 was applied to the neurofibromin fragment columns and washed with buffer A, and the bound CRMP-2 on each column was eluted by 2× SDS loading buffer. The eluted fractions were separated by SDS-PAGE, transferred onto PVDF membrane electrophoretically, and subjected to the immunoblotting analysis with anti-CRMP-2 antibody. To check the purity of thrombin-cleaved CRMP-2 and GST-neurofibromin fragments (GST-CSRD, -GRD, -CTD), each protein was subjected to SDS-PAGE and their patterns analyzed after staining with Simply Blue (Fig. 1*D*, *upper panel*).

Quantitative Western Blotting Analysis—After immunoblotting detection, the ECL patterns were scanned using LabScan 5.0 (GE Healthcare) with transparent mode and resolution 300 dpi, and Cy5 patterns were processed by fluorescence scanner Typhoon 9400. The intensities were measured using ProGenesis Work station version 2005 (PerkinElmer Life Sciences) or ImageQuant (GE Healthcare) with background subtraction and normalization by total spot volume mode. The intensity of each spot was recorded as digital data, and processed by Microsoft Office Excel. Experimental values are expressed as mean ± S.E. Paired Student's *t* test or one-way analysis of variance with Dunnett's test was used to identify significant differences where appropriate. *p* values of <0.05 were considered significant.

Cell Culture, Stimulation, Transfection, and Preparation of Cell Lysates—PC12 cells were cultured under 5% CO_2 at 37 °C in Dulbecco's modified Eagle's medium (Invitrogen) supplemented with 10% horse serum and 5% fetal bovine serum. Transfection into cells was performed with Lipofectamine 2000 (Invitrogen) according to the manufacturer's protocol. PC12 cells were stimulated with 50 ng/ml 2.5 S NGF (WAKO) for up to 72 h. For preparation of cellular lysates, cells were solubilized with NF1 lysis buffer (20 mM Tris-HCl, pH 7.5, 5 mM $MgCl_2$, 150 mM NaCl, 1 mM EDTA, 0.1% Nonidet P-40, 1 mM 4-(2-aminoethyl)-benzenesulfonyl fluoride hydrochloride, 1 μg/ml each aprotinin, pepstatin A, and leupeptin) and passed through a 25-gauge syringe 20 times. Lysates were centrifuged at 20,000 × *g* for 20 min at 4 °C, and the protein concentrations of

Downloaded from www.jbc.org at KUMAMOTO UNIV LIB on March 1, 2009

the supernatants were determined using the BCA protein assay (Pierce).

siRNA—Four target sequences for Rat NF1 siRNA were designed as follows: a 21-oligonucleotide siRNA duplex was designed as recommended elsewhere (9) and was synthesized by Gene Link (Japan) to target the rat NF1 sequence 5′-^{249}CAAGGAGTGTCTGATCAACTT-3′ (for 249 NF1 siRNA), sequence 5′-^{532}CTTCGGAATTCTGCTTCTGTT-3′ (for 532 NF1 siRNA), and sequence 5′-^{611}GGTTACAGGAGT-TGACTGTTT-3′ (for 611 NF1 siRNA). Annealing of the component strands of each siRNA and transfection were performed as described (9). FITC-labeled rat NF1 sequence (FITC-249 NF1 siRNA) was also synthesized by Gene Link. A 27-oligonucleotide siRNA duplex was designed and synthesized by iGENE therapeutics (Japan) to target the rat NF1 sequence 5′-GAAAGGGGCUUGAAGUUAAUGUCAAAG-3′. For control siRNAs, a 27-oligonucleotide siRNA duplex scramble sequence by iGENE therapeutics (Japan), and a double-stranded RNA targeting human *NF1* gene (5′-^{609}AACTTCG-GAATTCTGCCTCTG^{629}-3′) were used as a control.

Immunofluorescence Analysis—PC12 cells grown on a 35-mm culture dish were fixed with 4% paraformaldehyde in PBS for 15 min at room temperature and then permeabilized with 0.2% Triton X-100 in PBS for 15 min. After being washed with PBS, cells were incubated in primary antibodies diluted in PBS containing 0.2% bovine serum albumin, followed by a secondary antibody conjugated with a fluorescent dye for 60 min at room temperature, or the cells were incubated with rhodamine phalloidin to stain cellular actin for 60 min at room temperature. Analysis was performed with a confocal microscope (Fluoview, FV300, Olympus) or fluorescence microscope (with 20 × 1.6 Olympus IX71) (DPController, DPManager).

Time-lapse Video Analysis—Cells were placed on a collagen-coated glass-bottom plate with 6 wells (Iwaki). Dishes were maintained at 37 °C under 5% CO_2 in the chamber set under the camera, during the observation. Images were obtained using a 20× UPlan Apo objective (Olympus). The camera, shutters, and filter wheel were controlled by MetaMorph imaging software (Universal Imaging), and the images were collected every 5 min with exposure times of 100 ms. Through-focus z-series stacks consisting of three frames were acquired at each time point.

Two-dimensional Electrophoresis and Two-dimensional Difference Gel Electrophoresis (DIGE)—Mouse brain or PC12 cell lysates (10–50 μg), after desalting using two-dimensional-clean up kit (Amersham Biosciences), were mixed with 125 μl of rehydration solution (8 M urea, 0.5% (w/v) CHAPS, 0.2% (w/v) DTT, 0.5% (v/v) IPG buffer) and loaded into strip holders for first-dimension isoelectric focusing. IPG strips (pH 4–7) (Amersham Biosciences) were used and allowed to re-swell for 12 h. Strips were equilibrated in a two-step process in equilibration solution (2% SDS, 50 mM Tris-HCl, pH 8.8, 6 M of urea, 30% (v/v) glycerol, and 0.002% bromphenol blue) for 15 min each step. In step one, 1 mM DTT was added; in step two, 1 mM iodoacetamide was added. Strips were then subjected to two-dimensional SDS-PAGE (10% gel, 7 × 7 or 13 × 13 cm^2). The proteins separated in two-dimensional gels were stained with protein staining solutions or transferred onto nitrocellulose or PVDF membranes, and protein patterns were obtained using specific antibodies. The two-dimensional pattern images on the gels or membranes were visualized with fluorescence probes or ECL (GE Healthcare) and scanned by a confocal fluorescence scanner Typhoon 9400 (GE Healthcare).

For two-dimensional DIGE, mouse brain or PC12 cell lysates (10–50 μg) were labeled with 400 pmol of CyDye DIGE Fluor minimal dyes (GE Healthcare) freshly dissolved in anhydrous dimethylformamide. The labeling mixture was incubated on ice in the dark for 30 min, and the reaction was terminated by addition of 10 nmol of lysine. Equal volumes of 2× sample buffer (8 M urea, 4% (w/v) CHAPS, 2 mg/ml DTT, 1% (v/v) IPG buffer, pH 4–7) were added to each of the labeled protein samples. The two samples were mixed prior to isoelectric focusing by IPG strip and subjected to the two-dimensional PAGE as described above.

Staining of the Two-dimensional Gels by ProQuant Diamond Phosphoprotein Gel Stain and SYPRO Ruby Protein Gel Stain—For ProQuant Diamond staining, two-dimensional gels were fixed in 50% methanol containing 10% acetic acid once for 30 min and again for overnight. Gels were washed three times in water for 10 min and stained with ProQuant Diamond phosphoprotein gel stain (Invitrogen) in the dark for 60–90 min and then washed with destain solution (5% of 1 M sodium acetate, pH 4.0, containing 20% acetonitrile) three times for 30 min. Gels were washed twice with water for 5 min and scanned by Typhoon. For SYPRO Ruby gel staining, gels were fixed in 50% methanol containing 7% acetic acid for 30 min, stained in SYPRO Ruby protein gel stain (Invitrogen) for 3 h, and washed with 10% methanol containing 10% acetic acid for 30 min. The fluorescent images were scanned with Typhoon 9400, visualized, and processed as digital data with data mining software ImageQuant version 5.2, DeCyder (GE Healthcare), and ProGenesis Work station version 2005 (PerkinElmer Life Sciences).

RESULTS

The Identification of Neurofibromin C-terminal Associating Proteins—To isolate proteins that physically associate with neurofibromin, we used the C-terminal domain (CTD), one of the crucial regions in regulating neurofibromin function (10, 14), as a ligand. Mouse brain cytosolic lysates were loaded onto the affinity column with immobilized GST-CTD or GST. Associating proteins on both columns were eluted using high salt elution buffer. The concentration of eluted protein from the GST-CTD column was 3.7 times higher than that from the control column (Fig. 1*A*). To subject the proteins eluted from each column to iTRAQ analysis, each fraction was adjusted to the same protein concentration, separately trypsinized, and modified with four kinds of isobaric tags as follows: iTRAQ114 and -115 for control and iTRAQ116 and -117 for NF1-binding proteins. Four fractions modified with different iTRAQ tags were combined and subjected to NanoLC ESI QQTOF and NanoLC-MALDI-TOF-TOF analysis. The obtained MS/MS data were used for the identification of the specific CTD-associating proteins, and the iTRAQ tag ratio (116, 117 *versus* 114, 115) was calculated using ProQuant quantitatively.

Downloaded from www.jbc.org at KUMAMOTO UNIV LIB on March 1, 2009

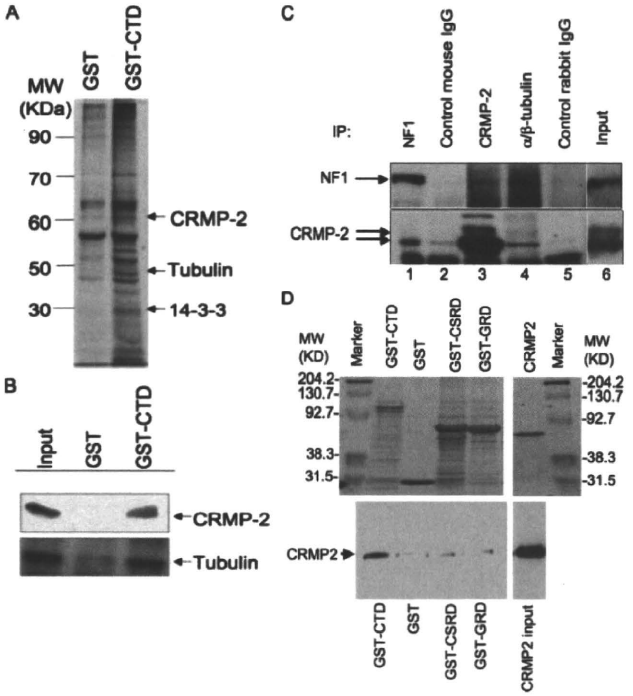

FIGURE 1. **Identification of neurofibromin-associating proteins.** *A*, silver staining of the associating proteins for the C-terminal domain of neurofibromin (GST-CTD) or those for the control (GST). Mouse brain proteins bound to the immobilized GST or GST-CTD are separated by SDS-PAGE and visualized with silver staining as described under "Experimental Procedures." The molecular mass markers are shown in kDa on the *left*, and *arrows* indicate the positions of the specific binding proteins identified. *B*, Western blotting analysis of identified proteins by the antibodies against CRMP-2 and tubulin. The eluted fraction from mouse brain proteins bound to immobilized GST or GST-CTD was immunoblotted with anti-CRMP-2 antibodies and anti-α-tubulin antibodies, followed by visualization with the ECL detection system. *C*, immunoprecipitation (*IP*) analysis of CRMP-2, tubulin α/β, and neurofibromin. Extracts of mouse brain in lysis buffer were incubated with anti-neurofibromin (*lane 1*), anti-CRMP-2 (*lane 3*), anti-tubulin α/β (*lane 4*) antibodies, and control anti-rabbit (*lane 2*) or mouse (*lane 5*) IgG antibodies for 3 h at 4 °C. The immunoprecipitates were analyzed by immunoblotting using the indicated antibodies (*upper panel*, anti-neurofibromin antibody; *lower panel*, anti-CRMP2 antibody) as described under "Experimental Procedures." *Input* (*lane 6*) shows the supernatant of the extract of mouse brain used for this study. *Arrows* indicate the position of the protein for neurofibromin (NF1) and CRMP-2 (*upper arrow*, phosphorylated form; *lower arrow*, nonphosphorylated form). *D*, direct binding of CRMP-2 to neurofibromin fragments *in vitro*. The GST fusion neurofibromin fragment proteins (GST-CSRD-(543–909), GST-GRD-(1168–1530), GST-CTD-(2260–2818)), GST, and CRMP2 (10 μg) purified from *E. coli* were separated with SDS-PAGE and stained with Coomassie Brilliant Blue (*upper panel*). Each of the GST fusion proteins (GST-CSRD, GST-GRD, and GST-CTD) and GST were immobilized on GSH-agarose beads and packed into each columns. Purified CRMP-2 protein (*upper panel, right photo*) was applied to the neurofibromin fragment columns and washed with buffer *A*, and the bound CRMP-2 on each column was eluted, subjected to SDS-PAGE (10%), and analyzed with Western blotting using anti-CRMP-2 antibody (*lower panel*) as described under "Experimental Procedures." The molecular mass markers are shown in kDa on the *left* and *right* in the *upper panel*, and an *arrow* indicates the positions of CRMP-2 identified in Western blotting.

At least 58 proteins having a specific high ratio of affinity to the GST-CTD compared with the GST column (an identification total ion score more than 61 and the best ion score confidence interval % more than 97%) were listed in Table 1. Identified proteins include not only the proteins previously found, such as neurofibromin-associating proteins 14-3-3s (14) and tubulins (13), but also many novel proteins not reported previously. The proteins were categorized into five main groups by their following biological functions: 1) cytoskeleton and its regulators, ARP2/3 complex 20-kDa subunit, actins, tubulins, and cofilin; 2) axonal outgrowth and guidance, collapsin-response mediator protein-2, CRMP-2/dihydropyrimidinase-related protein-2, and DRP-2, DRP-1; 3) neurotransmitter secretion, synapsin I and synaptojanin 1; 4) endocytosis, dynamin-1, protein kinase C, and casein kinase substrate in neurons protein 1; and 5) transcription translation regulator, EF1-α2, -γ, transcriptional activator protein PUR-α, SET protein, nucleosome assembly protein 1-like 1, and so on. Consistent with our interest in the function of neuronal cellular regulation associated to NF1 pathogenesis (6), we focused on CRMP-2, which showed one of the most significant associations in the GST-CTD column compared with those of control GST (Table 1).

To confirm that CRMP-2 is a neurofibromin-associating protein, the binding fractions of GST-CTD and control GST were separated by SDS-PAGE (10% polyacrylamide gel) and analyzed with silver staining (Fig. 1*A*) or immunoblotting using anti-CRMP-2 antibodies (Fig. 1*B*). CRMP-2 was significantly identified in the GST-CTD associating-protein fraction, although it was not obvious in that of the control GST fraction. Using the iTRAQ processing method, we detected 2.4 times higher CRMP-2 binding affinity (8.88 times higher CRMP-2 binding affinity: the ratio compensated with protein concentrations recovered from each column) in the GST-CTD fraction compared with the control GST fraction. The total ion score of identified 18 CRMP-2 peptides was 1437.

CRMP-2 and Tubulin Form a Complex with Neurofibromin in Vivo—CRMP-2, a tubulin-binding protein, has been known as a key molecule for axon guidance and is thought to form a protein complex whose effects on the regulation of microtubule formation in neuronal cells have not been completely identified (11). To confirm the association of CRMP-2 and tubulin to neurofibromin *in vivo*, the immunoprecipitates of the brain cytoplasmic protein fraction with antibodies against tubulin α and β, CRMP-2, and neurofibromin were analyzed by Western blotting (Fig. 1*C*). The interaction of tubulin was strong with the nonphosphorylated form of CRMP-2 (lower band for CRMP-2 in Fig. 1*C*), which is an active form and is increased in the intensity by the absence of phosphatase inhibitors, as reported (11), Interestingly, the binding of nonphosphorylated CRMP-2 to neurofibromin was significantly stronger than that of phosphorylated CRMP-2 (Fig. 1*C*). These results suggested that nonphosphorylated CRMP-2 forms a complex with neurofibromin as well as tubulin.

CRMP-2 Directly Binds to Neurofibromin C-terminal Domain—To analyze whether CRMP-2 binds directly to the neurofibromin or not, *in vitro* pulldown assay was performed with using recombinant CRMP-2 and GST-neurofibromin N-terminal center and C-terminal domain fragments. GST-CSRD-(543–909), GST-GRD-(1168–1530), GST-CTD-(2260–2818), or GST were immobilized on GSH-agarose beads and packed onto columns, and CRMP-2 protein was applied to each column. The bound CRMP-2 on each column was eluted and subjected to the Western blotting analysis using anti-CRMP-2 antibody. As shown in Fig. 1*D, lower panel*, CRMP-2 was detected in the eluates only from the GST-CTD column, suggesting that CRMP-2 could bind directly to the neurofibro-

Downloaded from www.jbc.org at KUMAMOTO UNIV LIB on March 1, 2009

TABLE 1
Neurofibromin-binding proteins identified with iTRAQ method

Protein name	Mass in Da	Peptide count[a]	Total ion score[b]	Best ion score C.I.[c] %	iTRAQ ratio average	S.E.[d]	Accession no.
Dihydropyrimidinase-related protein-2 (collapsin-response mediator protein 2 (CRMP-2))	67,393	18	1437	100	2.4	0.2	P47942
Nucleosome assembly protein 1-like	51,191	2	77	99.9	7.5	1.9	Q9Z2G8
Transcriptional activator protein PUR-α	38,003	5	331	100	6.4	0.9	P42669
Complement component 1, Q subcomponent binding protein, mitochondrial precursor	33,929	2	143	100	5.4	0.7	O35658
SET protein	36,844	3	247	100	5.3	0.7	Q63945
60 S ribosomal protein L22	17,558	2	85	100	4.3	0.9	P41104
Adapter-related protein complex 2 β1 subunit	114,363	2	74	99.9	3.5	1.4	Q9DBG3
Tubulin β chain	52,693	6	387	100	3.3	0.3	P04691
Tubulin β4 chain	52,138	4	322	100	3.2	0.4	Q9D6F9
Elongation factor 1-α	57,537	4	195	100	3.2	0.6	P62632
Tubulin α-2 chain	53,700	10	657	100	3.0	0.5	P05213
Synapsin I	74,486	4	201	100	2.9	0.8	O88935
Synaptojanin 1	186,358	2	135	100	2.8	0.6	Q8CHC4
Dynamin-1	106,354	3	141	100	2.8	0.3	P39053
Elongation factor 1-γ	55,271	4	164	100	2.8	0.7	Q9D8N0
Clathrin coat assembly protein AP180	99,365	2	68	99.9	2.7	0.5	Q05140
Hydroxyacylglutathione hydrolase (glyoxalase II)	32,482	2	115	100	2.7	0.8	Q99KB8
Guanine nucleotide-binding protein G(o), α subunit 1	44,389	2	74	99.9	2.5	0.3	P18872
Transcription factor A, mitochondrial precursor	33,008	2	62	99.7	2.5	0.3	Q91ZW1
Succinate semialdehyde dehydrogenase	57,424	2	89	100	2.5	0.7	P51650
Hexokinase, type I	118,767	4	168	100	2.5	0.4	P17710
Myelin basic protein	29,601	6	380	100	2.5	0.6	P04370
Transitional endoplasmic reticulum ATPase	96,894	2	79	100	2.4	0.2	P46462
Keratin, type I cytoskeletal 10	61,017	4	218	100	2.4	0.3	P02535
Microtubule-associated protein tau	87,172	2	108	100	2.3	0.4	P19332
Heat shock protein HSP 90-β (HSP 84)	94,427	8	519	100	2.3	0.3	P34058
Fumarate hydratase, mitochondrial precursor	59,614	2	131	100	2.3	0.5	P14408
Heat shock cognate 71-kDa protein	78,981	17	1092	100	2.3	0.2	P63018
Dihydropyrimidinase related protein-1 (Collapsin-response mediator protein 1 (CRMP-1))	67,542	3	384	100	2.3	0.5	Q62950
Actin, cytoplasmic 1 (β-actin)	44,934	9	526	100	2.3	0.1	P60710
Glyceraldehyde-3-phosphate dehydrogenase (GAPDH)	40,002	3	264	100	2.3	0.6	P04797
Heat shock protein HSP 90-α (HSP 86)	96,675	3	507	100	2.3	0.3	P07901
Nucleoside diphosphate kinase B	19,259	2	83	100	2.3	0.6	P19804
Malate dehydrogenase, mitochondrial precursor	39,632	3	155	100	2.3	0.2	P08249
Hemoglobin α chain	16,731	5	218	100	2.2	0.4	P01942
Protein kinase C and casein kinase substrate in neurons protein 1	57,082	4	226	100	2.2	0.2	Q61644
Serine/threonine protein phosphatase 2A, catalytic subunit, β isoform	37,852	2	76	99.9	2.1	0.3	P62715
Vacuolar protein sorting 35	99,082	2	141	100	2.1	0.4	Q9EQH3
Stress-70 protein, mitochondrial precursor	81,549	2	75	100	2.1	0.4	P38647
SH3-containing GRB2-like protein 2	44,202	4	330	100	2.1	0.3	Q62420
ARP2/3 complex 20 kDa	21,786	2	61	97.9	2.1	0.4	P59999
Glutamine synthetase	45,829	6	353	100	2.0	0.2	P15105
Hemoglobin β-1 chain	17,542	4	279	100	2.0	0.2	P02088
Osmotic stress protein 94	105,985	3	197	100	2.0	0.2	P48722
Aspartate aminotransferase, mitochondrial precursor	52,248	2	138	100	2.0	0.4	P05202
L-Lactate dehydrogenase A chain	40,721	4	270	100	1.8	0.3	P06151
Malate dehydrogenase, cytoplasmic	40,961	5	342	100	1.8	0.1	P14152
Aldehyde dehydrogenase, mitochondrial precursor	61,482	5	284	100	1.8	0.2	P47738
Creatine kinase, ubiquitous mitochondrial precursor	50,111	3	252	100	1.7	0.2	P30275
Ubiquitin-activating enzyme E1	126,857	3	141	100	1.7	0.7	Q02053
78-kDa glucose-regulated protein precursor	81,426	4	165	100	1.7	0.1	P20029
Heat shock 70-related protein APG-2	106,832	8	484	100	1.7	0.1	Q61316
Ferritin heavy chain	23,111	2	88	100	1.7	0.2	P09528
14-3-3 protein β/α	31,046	2	523	100	1.7	0.2	P35213
14-3-3 protein ε	32,064	5	407	100	1.7	0.1	P62260
4-Aminobutyrate aminotransferase, mitochondrial precursor (GABA aminotransferase)	61,567	2	87	100	1.7	0.1	P61922
Aspartate aminotransferase, cytoplasmic	49,383	5	250	100	1.7	0.1	P05201
Glutamate dehydrogenase, mitochondrial precursor	66,775	11	631	100	1.6	0.1	P10860

[a] Peptide count represents number of peptides using iTRAQ quantitation.
[b] Total ion score represents confidences of protein identification.
[c] Best ion score C.I. % represents confidences of protein identification and MS/MS spectrum.
[d] S.E. represents standard error of iTRAQ ratio average.

min C-terminal domain without intermediate proteins such as tubulin or other binding proteins that were identified in this study.

Neurofibromin Is Co-localized with CRMP-2 in the Distal Tips of Neurites in Differentiated PC12 Cells—To demonstrate the localization of neurofibromin in differentiated PC12 cells, after NGF treatment of the cells we examined the expression pattern of neurofibromin immunocytochemically using anti-NF1 antibody. As shown in Fig. 2, neurofibromin was significantly distributed throughout the cells, being found in the perinucleus, the cytoplasm, and the apical region of neurites (Fig. 2*A*). To further confirm the co-localization of neurofibromin and CRMP-2 in differentiated PC12 cells, we analyzed the expression patterns of both CRMP-2 and neurofibromin using both anti-NF1 and anti-CRMP-2 antibodies. As we expected, CRMP-2 was found to be co-localized with neurofibromin in

Downloaded from www.jbc.org at KUMAMOTO UNIV LIB on March 1, 2009

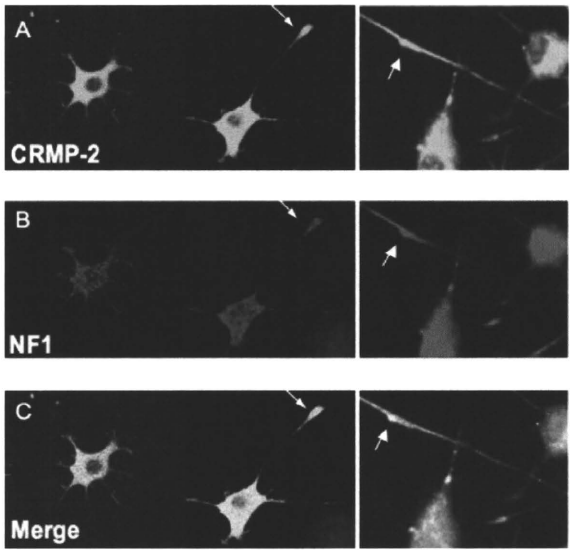

FIGURE 2. **Co-localization of neurofibromin and CRMP-2 in differentiated PC12 cells.** PC12 cells with NGF stimulation were detected by rabbit anti-NF1 (4 μg/ml) (*B* and *C*) and mouse anti-CRMP-2 antibodies (5 μg/ml) (*A* and *C*), and followed by Alexa 568-conjugated anti-rabbit IgG antibody (*red*), and Alexa 488-conjugated anti-mouse antibody (*green*), respectively, as described under "Experimental Procedures." The co-localization was shown in the merged image (*C*) with *yellow color*. Cells were observed by a confocal microscope (Fluoview, FV300, Olympus) or fluorescence microscope (with 20 × 1.6 OLYMPUS IX71) (DPController, DPManager). The *arrows* point to regions of neurofibromin and CRMP-2 co-localization in the distal tips and branches along the neurites. The results were reproducible in five experiments performed with independent preparations.

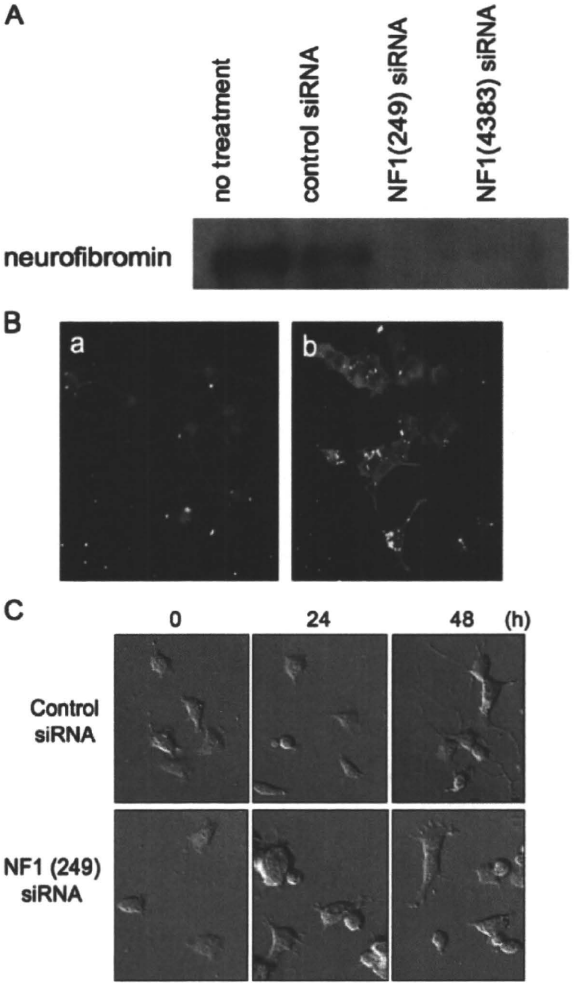

FIGURE 3. **Effects of the NF1 siRNA on neurite outgrowth of PC12 cells.** *A*, immunoblot analysis of whole cell lysates extracted from PC12 cells, transfected with siRNA for NF1(249), NF1(4383), or control siRNA. Cells were harvested after 48 h of NF1 siRNA or control siRNA transfection and analyzed by immunoblotting with the anti-neurofibromin antibodies. *B*, suppression of NF1 expression leads to changes in neurite outgrowth of PC12 cells. Cells were fixed and reacted with rhodamine phalloidin to stain actins after 48 h of transfection of FITC-NF1(249) siRNA, and observed with the confocal fluorescent microscope. The *red fluorescence* shows actin dynamics, and the *green* or *yellow fluorescences* (merged with actin) show FITC-NF1 siRNA incorporated into the perinuclear space with a specific manner (*b*) or attached on the cellular surface with nonspecific manner (*a*). *C*, representative images of time-lapse video analysis of PC12 cells transfected with NF1 siRNA or control siRNA; PC12 cells were transfected with NF1(249) siRNA or control siRNA, stimulated with NGF, and analyzed by time-lapse. The images show the morphology of PC12 cells transfected with NF1 siRNA (*lower panel*) or control siRNA (*upper panel*) at 0, 24, and 48 h after NGF treatment.

the cytoplasmic region and neurites, especially in the distal tips and the cylinder of neurites where CRMP-2 and microtubules form the center core (*indicated with white arrows* in Fig. 2, *A–C*). In addition, neurofibromin is particularly expressed in the adhesive membranous site in the neurite distal cone being linked to the core of CRMP-2 and microtubules of PC12 cells. These results demonstrate that neurofibromin and CRMP-2 are co-localized in PC12 cells, especially in the growing neurites during the differentiation of cells, indicating that the interaction of these molecules may influence the regulation of neurite outgrowth in PC12 cells.

The Effects of NF1 siRNA on the Neurite Outgrowth of PC12 Cells after NGF Treatment—To analyze how NF1 functions during neurite outgrowth regulation in association with CRMP-2 after NGF stimulation, knockdown of neurofibromin by NF1 siRNA in PC12 cells was performed, and the phenotypic change of the neurite outgrowth compared with that of the control siRNA transfected cells was then observed. After 48 h following transfection with NF1(249) siRNA or NF1(4383) siRNA, a more than 90% depletion of neurofibromin in PC12 cells was confirmed with Western blotting using anti-NF1 antibody (Fig. 3*A*). Morphological changes of cellular neurite outgrowth after transfection with NF1 siRNAs were precisely analyzed using confocal microscope and time-lapse microscope video analysis. Interestingly, compared with the control cells, which showed normal neurite outgrowth, significant inhibition of neurite outgrowth in PC12 cells was observed after transfection of all types of the NF1 siRNA (Fig. 3, *B* and *C*, supplemental Fig. S1, and supplemental movies 1 and 2). As shown in Fig. 3*B*, *panels a* and *b* (supplemental Fig. S1*A–C*), cells that incorporated fluorescent NF1 siRNA into the peri-nuclear region showed significant inhibition of neurite outgrowth. In contrast, cells that failed to uptake NFI siRNA and cells with NF1 siRNA attached to the cellular surface in a nonspecific manner showed normal neurite outgrowth. This retraction of neurites was detected reproducibly with time-lapse microscope video analysis (Fig. 3*C* and supplemental movies 1 and 2). Especially after 24–48 h of NF1 siRNA transfection, the neurite retraction (collapse) was significantly compared with the control cells in a time-dependent manner (Fig. 3*C*). These results strongly indi-

Downloaded from www.jbc.org at KUMAMOTO UNIV LIB on March 1, 2009

cate that neurofibromin is required for neurite outgrowth in PC12 cells, and they suggest that the interaction of neurofibromin and CRMP-2 plays an important role in neurite outgrowth in PC12 cells.

Proteomic Differential Analysis between PC12 Cells Treated with NF1 siRNA and Control siRNA by Two-dimensional Fluorescence DIGE—To study the precise differences in protein expression patterns between NF1 siRNA-transfected and control cells, proteomic analysis by two-dimensional fluorescent DIGE was performed. Before analysis, the cell lysates from NF1 siRNA-transfected PC12 cells and control cells were labeled with Cy5-fluora and Cy2-fluora, respectively, and then mixed into one fraction and subjected to two-dimensional PAGE using a 13-cm IPG strip (pI 4–7) for the first dimension, and SDS-PAGE (10%, 13 × 13 cm) for the second dimension of electrophoresis. The two-dimensional images were obtained after scanning with two fluorescent Cy5 and Cy2 filters and analyzed with inferred from direct assay. More than 1,000 protein spots obtained in each scan (control, 1,071 spots; NF1 siRNA, 1,060 spots) were reproducibly detected in each sample (Fig. 4*A*). For over 100 spots, the intensity varied by a factor of more than 1.5 between NF1 siRNA-transfected cells and control cells. Similar results were obtained from another set of two-dimensional DIGE gels for which the Cy2/Cy5 labeling was switched (data not shown).

Among these spots, at least seven differently expressed CRMP-2 proteins were identified in two-dimensional DIGE and two-dimensional Western analysis (Fig. 4, *A–C*). Four major spots for CRMP-2, spots 1–4, appear from right to left (pI 6.0-5.4), and three minor spots, spots 1.5, 2.5, and 3.5, appear between spots 1 and 2, spots 2 and 3, and spots 3 and 4, respectively (Fig. 4*B, lower panel*). Interestingly, the intensity of spot 1 was significantly decreased (*red* (siNF1)/*green* (control) = 0.3) after NF1 siRNA transfection (Fig. 4*B, upper panel*). For confirmation, the two-dimensional Western pattern of CRMP-2 was semi-quantitatively analyzed using PC12 cell lysates with several conditions. As shown in Fig. 4, *C–E*, the time course analysis after NGF treatment showed that the ratio of spot 1 intensity to total spot intensity was significantly decreased in a time-dependent manner compared with the control cells. We also observed changes in the intensities of the other spots corresponding to CRMP-2 (spots 1.5, 2, 3, and 4) (Fig. 4*C*). In particular, the ratio of spot 1.5 intensity to total spot intensity was increased significantly after NGF stimulation in NF1 siRNA-transfected cells. These results suggested that changes in the spot intensities of CRMP-2 spots may represent changes in the modification status, such as phosphorylations, as well as NF1-related regulation of neurite outgrowth in PC12 cells.

The Effects of NF1-GRD Type I Overexpression in NF1 siRNA-Treated PC12 Cells—To confirm whether the changes in neurite phenotypes and CRMP-2 spot patterns in two dimensions were caused by the suppression of neurofibromin with NF1 siRNA, an expression plasmid corresponding to NF1-GRD type I was transfected to PC12 cells in the presence or absence of NF1 siRNA after NGF treatment. Overexpression of GRD type I, which possesses strong RAS-GAP activity (6), significantly effected to rescue both neurite retraction and CRMP-2 spot shifts, especially the intensities of spot 1 and spot 1.5, which were returned to the control (not treated with NF1 siRNA) levels, in PC12 cells (Fig. 5, *A* and *B*). These results demonstrate that the neurite outgrowth of PC12 cells needs neurofibromin GAP activity and that these phenotypic changes are correlated with the CRMP-2 protein spot shifts.

Analyses of CRMP-2 Phosphorylation Patterns in Two-dimensional DIGE—CRMP-2 has been known as a highly phosphorylated protein in neuronal cells (16). To determine whether each spot corresponding to CRMP-2 was the phosphorylated form or not, we analyzed phosphorylated proteins in PC12 cells by two-dimensional DIGE using phospho-specific protein stainer, ProQuant Diamond. Fig. 6*A* (*lower panel*) shows that ProQuant Diamond staining of spots 1.5, 2, 2.5, 3, 3.5, and 4 was obvious (*yellow* or *orange*), whereas spot 1 was unresponsive to the staining (*green*). This evidence was confirmed with another experiment using Cdk inhibitors that amplify spot 1 with protein (SYPRO Ruby) level but not phosphorylation (ProQuant Diamond) level (supplemental Fig. S2). These results indicated that, among the seven CRMP-2 spots in the two-dimensional gels, only spot 1 represents the nonphosphorylated form, whereas the other spots are phosphorylated forms of CRMP-2. Semi-quantitative analysis of spot intensities by ProQuant staining revealed that specific phosphorylation levels in each protein spot were increased in correlation with decreases in spot pI (Fig. 6*B*). These results suggest that the shift of protein spots from right to left (from pI 5.9 to pI 5.4) reflects the differences in phosphorylation levels of each spot. The specific phosphorylation/protein levels of spots 1.5 and 2 were similar, although the pI of each spot showed a small difference, suggesting that these spots possess the same level of phosphorylation but different phosphorylation sites. Spots 2.5 and 3 also showed similar levels of specific phosphorylation when compared with each other but almost twice the level when compared with the pair of spots 1.5 and 2. This indicated that spots 2.5 and 3 possess different phosphorylation sites and 2 times higher levels of phosphorylation than spots 1.5 and 2.

Identification of the CRMP-2 Phosphorylation Sites in PC12 Cells by Two-dimensional Western Analysis—To identify the phosphorylation sites of CRMP-2 proteins, whose spots were differentially shifted forming a seven-spot pattern (Fig. 7*A*), we analyzed the phosphorylation patterns of CRMP-2 in PC12 cells by Western blotting in several conditions of kinase inhibitors using specific antibodies against phosphorylated CRMP-2. After calyclin A treatment to increase the CRMP-2 phosphorylation levels in PC12 cells (Fig. 7*B*), significant disappearance of CRMP-2 spots 1.5, 2.5, and 3.5 was observed in the presence of the Rho kinase inhibitor (Y27632) (Fig. 7*C*). A specific antibody against the Rho kinase-phosphorylated CRMP-2 (anti-phospho-Thr^{555} CRMP-2 antibody) reacted with those spots (Fig. 7*D*), whereas in the presence of Y2763, these positive spots all disappeared (Fig. 7*E*), suggesting that spot 1.5 could be Thr^{555}-phosphorylated CRMP-2 by Rho kinase and that spots 2.5 and 3.5 could have other phosphorylation sites in addition to Thr^{555}. The specific antibody against GSK-3β-phosphorylated CRMP-2 (anti-phospho-Thr^{514} CRMP-2 antibody) reacted with spots 3 and 4 significantly (Fig. 7*K*). In the presence of GSK-3β inhibitor (LiCl), spots 3 and 4 shifted and displayed

The Journal of Biological Chemistry ASBMB jbc

Downloaded from www.jbc.org at KUMAMOTO UNIV LIB on March 1, 2009